

D I S S E R T A T I O N

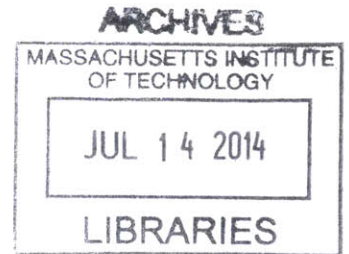
Hologvideo *on a* Stick:

Integrated Optics for Holographic Video Displays

by

Daniel E. Smalley

B.S. Massachusetts Institute of Technology 2005
M.Eng Massachusetts Institute of Technology 2005
M.S. Massachusetts Institute of Technology 2008



Submitted to the Program in Media Arts and Sciences,
School of Architecture and Planning,
in partial fulfillment of the requirements for the degree of
Doctor of Philosophy in Media Arts and Sciences
at the

MASSACHUSETTS INSTITUTE OF TECHNOLOGY

September, 2013

© Massachusetts Institute of Technology 2013. All rights reserved.

Author

Signature redacted

Program in Media Arts and Sciences
August, 2013

Certified by

Signature redacted

V. Michael Bove, Jr.
Principal Research Scientist
Thesis Supervisor

Accepted by

Signature redacted

Pattie Maes
Associate Academic Head
Program in Media Arts and Sciences

A B S T R A C T

Holovideo *on a* Stick:

Integrated Optics for Holographic Video Displays

by

Daniel E. Smalley

Submitted to the Program in Media Arts and Sciences,
School of Architecture and Planning,
in partial fulfillment of the requirements for the degree of
Doctor of Philosophy

Abstract

In this dissertation I describe the development of a new integrated-optics platform for holographic video consisting of arrays guided-wave acousto-optic devices. This platform serves as the foundation for a new family of holographic video architectures that trade off its enormous pixel bandwidth for display extent, view angle and frame rate. This dissertation work demonstrates how techniques from the fields of integrated optics and integrated acoustics can be brought to bear on the challenges of holographic projection and display (for example, how to meet the large pixel requirement of holography while constraining cost and complexity). This work demonstrates devices built from this platform which include novel features such as: polarization rotation via mode-coupling; wavelength division multiplexing of red, green and blue signals; high total pixel bandwidth; continuous horizontal parallax and extremely low cost of construction relative to comparable displays.

Thesis Supervisor: V. Michael Bove, Jr.

Title: Principle Research Scientist

R E A D E R S

Signature redacted

Thesis Supervisor.

.....
V. Michael Bove, Jr.
Principal Research Scientist
Director, Consumer Electronics Laboratory
Thesis Supervisor

Signature redacted

Thesis Reader

.....
Ed Boyden
Associate Professor of Media Arts and Sciences
Benesse Career Development Professor of Research in Education

Signature redacted

Thesis Reader

.....
Rajeev Ram
Professor of Electrical Engineering
Department of Electrical Engineering and Computer Science
Associate Director, Research Laboratory of Electronics



For Pamela, Neal, Jeffrey and Baby Anne

A C K N O W L E D G E M E N T S



My Advisor, [Dr. Bove](#), has been involved in this work from the very beginning. Not only has he been very patient during periods of slow progress but he has also, on several occasions, given advice that has changed the course of this research for the better. I could not have hoped for a more helpful or understanding advisor.



[Elroy Pearson](#) invited me out to MIT to participate as an undergraduate researcher after we corresponded briefly about some holography experiments I was conducting in my garage. That experience introduced me both to the Media Lab and to holographic video and set me on my current research path. If it weren't for Elroy, I might still be turkey farming in rural Utah.



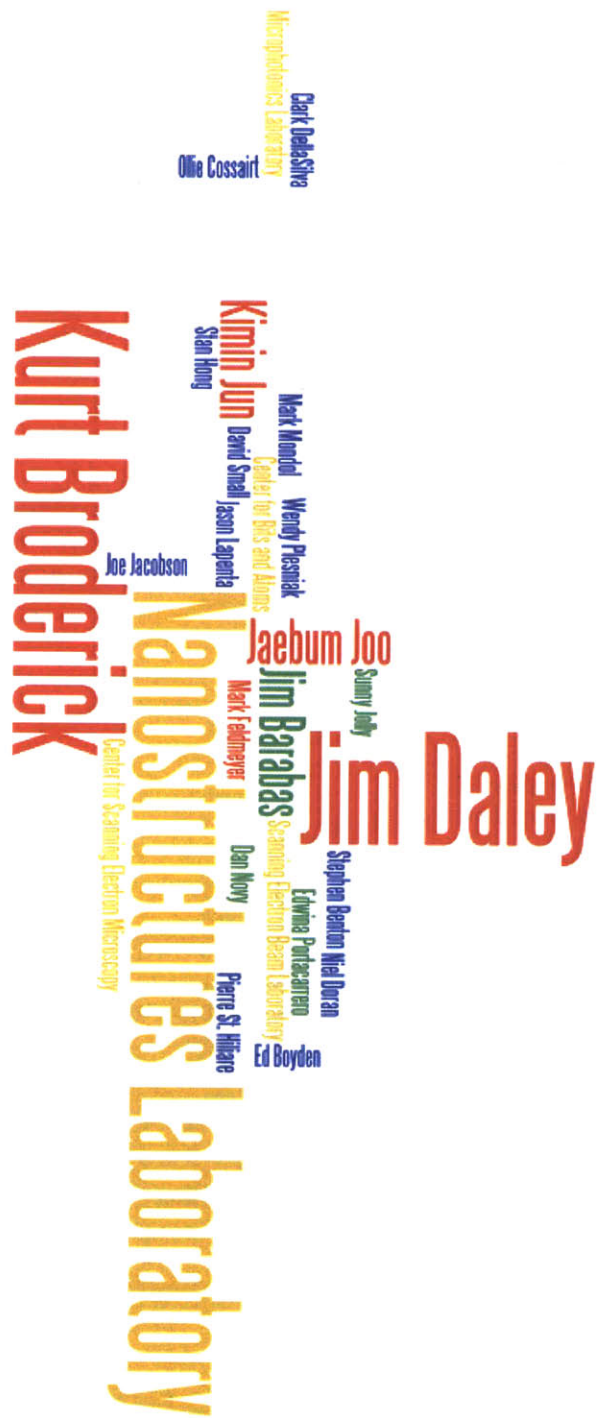
[Quinn Smithwick](#) gave some of the best years of his life to our holovideo effort and deserves a lot more recognition that he has received to date (even considering the temporary shrine we erected to him in our office after he left for Disney). I'm grateful that I had someone who as talented as Quinn working with me during the toughest parts of this research and grateful for the notebooks of ideas that our discussions generated over the years.



At the Media Lab your origin is of no importance.
What counts is the power of your ideas.



-Kristin Hall



This research was supported by Intel Corporation. Also, Nvidia provided equipment for the prototypes used in this dissertation.

C O N T E N T S

Introduction

Background

Guided Wave Modulators	16
Advantages	18
Previous Modulator Work	21
Previous Geometry Work	22
Summary	23

Theory

Piezoelectric Materials	26
Interdigital Transducers	27
Waveguides	29
Mode Coupling	30
The Grating Equation	34

Design

Decision Tree	40
Transducer Dimensions	46
Bandwidth Budget	48
Design Steps	48
Examples	54
Design Summary	54
Electrical Path	56
Optical Path	58
Software Path	60

Fabrication

Waveguide Fabrication	66
Package	70
Display Fabrication	72
Completed Display	75

Results

Test Patterns	80
Output Images	80
Wavelength Division Multiplexing for Color	82

Conclusion

Holovideo Display	88
Future Work	89

Appendix

Holovideo Card	92
Horizontal Controller Card	94
Vertical Scanner Controller	96

Bibliography


F I G U R E S

Figure 2-1	Pixel artifacts	16
Figure 2-2	Single channel modulator	17
Figure 2-3	Multiple channel modulator	17
Figure 2-4	Fabricated modulator	17
Figure 2-5	Polarization rotation	19
Figure 2-6	Angular deflection	19
Figure 2-7	Collinear vs. normal illumination	20
Figure 2-8	Frequency multiplexing of color	21
Figure 2-9	MIT Mark I Holovideo display	22
Figure 3-1	Waveguide modes	31
Figure 3-2	K-space view of waveguide modes	31
Figure 4-1	Waveguide modulator decision tree.	41
Figure 4-2	Design summary for waveguide device.	47
Figure 4-3	Index profile.	48
Figure 4-4	SAW Velocities.	48
Figure 4-5	SAW Velocities.	49
Figure 4-6	Optical power density.	49
Figure 4-7	Display design steps (facing page)	50
Figure 4-8	Large and small example display geometries	57
Figure 4-9	Signal path for holovideo monitor electro-optics.	59
Figure 4-10	Holographic video monitor optical path	61
Figure 4-11	Holographic video monitor internals	63
Figure 5-1	Proton exchange of waveguides	67
Figure 5-2	Lift-off of aluminum transducers	67
Figure 5-3	A single, chirped transducer	71
Figure 5-5	A completed guided-wave modulator	71
Figure 5-4	Eighteen chirped transducers	71
Figure 5-6	Construction of the holographic video monitor (facing page)	72
Figure 5-7	The first completed holographic video monitor prototype	75
Figure 6-1	Design parameters vs. measured parameters (facing page)	78
Figure 6-2	A test of channel width vs. diffraction efficiency (facing page top)	80
Figure 6-3	A test of waveguide loss vs. proton exchange time and annealing(facing page bottom)	80
Figure 6-4	Test of the telescope demagnification	82
Figure 6-5	Test of image descan	82
Figure 6-6	Test of the polarization rotation	82
Figure 6-7	One view of a reconstructed holographic stereogram.	83
Figure 6-8	Close up of a monochrome holographic stereogram	83
Figure 6-9	Frequency response for device used in holographic video monitor	84
Figure 6-10	Demonstration of frequency division color control	84
Figure 6-11	Crosshairs used to align the three color images	84
Figure 6-12	Full color holographic stereogram	85
Figure 6-13	Close up of color stereogram	85

1

Introduction

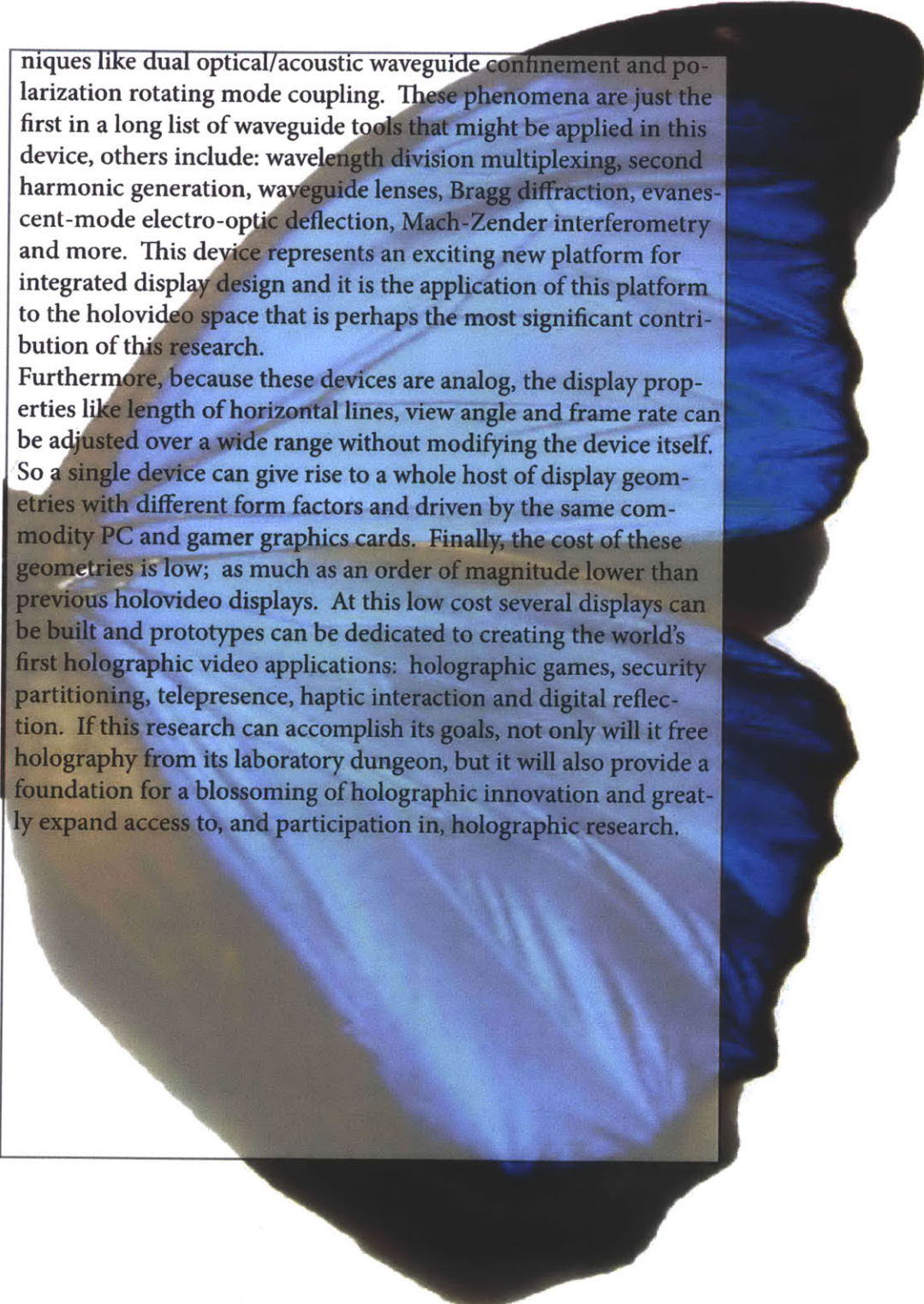
I N T R O D U C T I O N



Shortly after I first arrived at the Massachusetts Institute of Technology (MIT), nearly a decade ago, I was introduced to the storied Mark II holographic video display. It was (and to a great extent, still is) a sprawling array of scanning mirrors and lenses. It boasted the two largest tellurium dioxide crystals ever grown. It was driven by a custom built supercomputer and a six-foot rack of radio frequency (RF) electronics. Remarkably, all this hardware was dedicated to producing a monochrome, 144-line image no larger than a postcard—but what an image! This was a true holographic image. Not an anaglyph or mere stereogram but a faithfully reconstructed holographic image with motion parallax and accommodation cues. Not only did this display have the ability to control the direction of light, but also the remarkable and rare ability to mold its curvature. I fell in love. I swore that I would one day have a holovideo display of my very own; and the result of that vow is this dissertation.

A fully realized holographic video display is a wondrous thing to contemplate. Holographic displays can faithfully reproduce the iridescence of a butterfly's wing and the warping of images through glass and water. Two people viewing a holographic video display can be made to see entirely different images. It is possible that one day holographic displays will adapt to the eyeglass prescription of their viewers or image through turbulent media. However, it is unlikely that any of these things will happen until holography can be released from the bondage of the darkened basement laboratory and freely dispersed among artists, engineers and designers as a tool for creative exploration. Up until now, holographic video displays have been both costly and complex. We need a display that is simple and inexpensive.

This dissertation will describe the development of a holographic video display that is not only inexpensive and parsimonious, but also teeming with innovative potential. This display has at its heart a custom designed integrated optics device, which employs tech-



niques like dual optical/acoustic waveguide confinement and polarization rotating mode coupling. These phenomena are just the first in a long list of waveguide tools that might be applied in this device, others include: wavelength division multiplexing, second harmonic generation, waveguide lenses, Bragg diffraction, evanescent-mode electro-optic deflection, Mach-Zender interferometry and more. This device represents an exciting new platform for integrated display design and it is the application of this platform to the holovideo space that is perhaps the most significant contribution of this research.

Furthermore, because these devices are analog, the display properties like length of horizontal lines, view angle and frame rate can be adjusted over a wide range without modifying the device itself. So a single device can give rise to a whole host of display geometries with different form factors and driven by the same commodity PC and gamer graphics cards. Finally, the cost of these geometries is low; as much as an order of magnitude lower than previous holovideo displays. At this low cost several displays can be built and prototypes can be dedicated to creating the world's first holographic video applications: holographic games, security partitioning, telepresence, haptic interaction and digital reflection. If this research can accomplish its goals, not only will it free holography from its laboratory dungeon, but it will also provide a foundation for a blossoming of holographic innovation and greatly expand access to, and participation in, holographic research.

I N T R O D U C T I O N

2

Background

B A C K G R O U N D

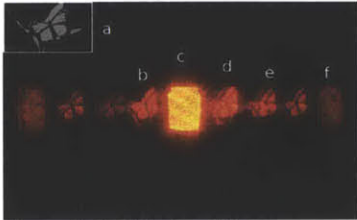


Figure 2-1 Pixel artifacts
Holographic stereogram artifacts from a pixelated, Liquid Crystal on Silicon (LCoS) modulator. (a) the stereogram mask (b) the desired output (c) zero order, unmodulated and undiffracted light (d) undesired conjugate image (e) high frequency orders and quantization noise (f) orders arising from the pixel structure of the modulator

The limitations and affordances of holographic video displays are chiefly dictated by the spatial light modulators (SLMs) upon which they are built. The temporal bandwidth of the spatial light modulator determines the display size, view angle (because higher pixel densities lead to higher angles of diffraction), and frame rate. The pixel pitch determines the angle of the display or the power of the lenses needed to achieve a wide view angle. The space-bandwidth product, which is related to the numerical aperture of the holographic grating, determines the maximum depth range and number of resolvable views the display will possess. Finally, the optical nonidealities of the modulator give rise to noise and artifacts in the display output. State-of-the-art technologies for spatial light modulation (e.g., liquid crystal (LC), micro-electro-mechanical systems (MEMS) [6], [7], and bulk-wave acousto-optic modulators [21] have proven challenging to employ in holographic video displays¹. Before using these modulators in a holographic display, one must address their low bandwidth, low diffraction angle, quantization error, the presence of zero and other order noise and deal with the spatial or temporal multiplexing of color (see Figure 2-1). Much of the cost and complexity of modern holographic displays is due to efforts to compensate for these deficiencies by adding eye tracking to deal with low diffraction angle [8], duplicating and phase shifting the optical path to eliminate the zero order [9], or creating large arrays of spatial light modulators to increase the display size [10]. The cost and complexity of holographic video displays could be greatly reduced if a spatial light modulator could be made to have better affordances than the LC and MEMS devices currently employed.

GUIDED WAVE MODULATORS

I have developed a spatial light modulator based on anisotropic leaky-mode coupling which brings the tools of guided wave optics to bear on the challenges of holographic video and possesses many advantages over LC and MEMS devices when applied to holographic video display. Here, I describe how the device can be fabricated inexpensively and made to support an aggregate temporal band-

¹ Not mentioned here are a number of SLMs that might be considered for holographic video in the future including EO waveguide phased-arrays (currently operating in infra-red region)[33] and magneto-optic modulators[34].

width of more than 50 Gpixels/sec--an order of magnitude increase over the current state-of-the-art. I also demonstrate a three-fold increase in angular deflection over other modulator technologies due to the edge-lit nature of the waveguide grating structure and the resulting increase in space-bandwidth product. The modulator exploits guided-wave phenomena, most notably anisotropic mode conversion for the elimination of zero-order light and tunable wavelength filtering for the simultaneous and superimposed modulation of color signals.

My multichannel modulator was inspired by similar devices that have been used in the telecom industry for decades where bandwidth is of prime importance. My devices were designed specifically to meet the needs of advanced 3D displays by employing techniques and technologies from integrated optics and acoustics. Multichannel leaky-mode devices were first theoretically described by Proklov who intended them for use in multi-channel spectrum analyzers and as optical multiplexer/demultiplexers [14]. He later fabricated a single channel spectrum analyzer as proof of concept. Tsai later reproduced Proklov's experiments in proton exchanged waveguides rather than titanium indiffused waveguides, also single channel, to achieve higher output efficiencies and described the devices as a general scanning solution. Finally, Ito, fabricated a wide single channel device which he intended to investigate as a technology for steering the laser on the reading head of an optical disk drive[15]. My research has been the first to propose guided wave acousto-optics as a solution for holovideo and will be the first to fabricate single and multiple channel leaky-mode devices for this purpose.

Structurally, an anisotropic leaky-mode coupler is a proton-exchanged [11] channel waveguide on a lithium niobate substrate with a transducer at one end [12], [13]. The waveguide is anisotropic and only guides light in one polarization. When excited by an RF signal, the transducer generates surface acoustic waves [10] that propagate collinearly with the light trapped in the anisotropic waveguide (see Figure 2-2). When the phase-matching condition is met the acoustic pattern, encoded with holographic information, couples the guided light into a leaky mode of orthogonal polariza-

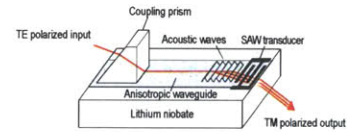


Figure 2-2 Single channel modulator

Guided, TE polarized light interacts with surface acoustic waves (SAW) which convert it into leaky TM polarized light (note that TM to TE coupling is also possible in Z-cut lithium niobate). The acoustic pattern acts as the holographic diffraction pattern and can cause the output to scan, focus, or form a wavefront that will become part of a holographic image.

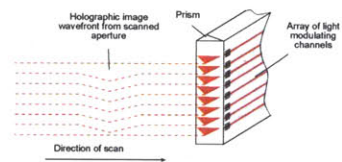


Figure 2-3 Multiple channel modulator

The holographic image is formed by scanning the aperture of the anisotropic waveguide device having one or more channels.

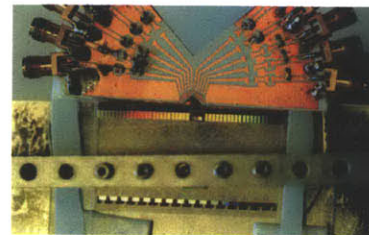


Figure 2-4 Fabricated modulator

tion which then exits the waveguide-substrate interface. The index contrast of the waveguide-air interface is much higher than that of the waveguide-substrate interface; this asymmetry of boundary conditions means that there is no conjugate image (i.e. no upward output beam). This leaky mode emits a wavefront-modulated fan of light that exits one face of the wafer and forms part of a holographic output image. Each channel waveguide writes one or more lines of the output and several channels can be fabricated next to each other to create large aggregate bandwidths suitable for large display size and resolution (see Figure 2-3). Such a fabricated multichannel device is shown in Figure 2-4.

Guided wave modulators are made by patterning a hard mask of silicon dioxide on lithium niobate wafer and then exposing it to an acid to get proton exchange. This creates a waveguide on the surface of the wafer. Next, a standard liftoff process is used to pattern interdigital aluminum transducers on or near the entry to the waveguide. When the transducers are excited by an RF signal they will essentially ‘pinch’ the surface of the wafer via the piezoelectric effect and cause a stream of surface acoustic waves that will propagate along the length of the waveguide. This stream is effectively a one dimensional holographic fringe pattern. Light trapped in the waveguide interacts with the acoustic wave and is converted from a guided mode of one polarization to a leaky mode^{4,5} of an orthogonal polarization. This output light is a holographic image that results from diffraction off of the acoustic fringe pattern.

ADVANTAGES

Anisotropic leaky-mode couplers possess several advantages over other spatial light modulators used for holographic video (see Table 1). In addition to being simple to fabricate and drive, they are capable of high deflection for a given pixel pitch and can leverage tools from guided-wave optics to address noise and color multiplexing.

affordance	pixelated modulators	anisotropic waveguide modulators
temporal bandwidth	5 gigapixels/sec. (8 megapixels)	50 gigapixels/sec. (500 channels)
output angle ($\lambda=532$ nm, $\Lambda=12$ μ m)	2.54 degrees	24.7 degrees
output polarization orthogonal to zero order	no	yes
fabrication complexity	10-20 mask steps	2 mask steps
superfluous conjugate mode	yes	no

Table 2-1 Advantages of waveguide modulators

The advantages of anisotropic waveguide modulators over pixelated spatial light modulators.

Modulators with a defined pixel structure and a backplane (e.g., LC and MEMS devices) become more complex as pixels are added which constrains scalability. Bulk-wave acousto-optic modulators can produce the acoustic equivalent of 100 million pixels per second per acoustic channel; however, channels cannot be placed too closely together because of the resulting acoustic crosstalk. Anisotropic leaky mode couplers enjoy lateral guidance of the acoustic wave which makes it possible for adjacent channels to be placed tens of microns apart and for hundreds of channels to be placed side-by-side on a single substrate thereby providing aggregate bandwidths in excess of 50 billion pixels/sec. This bandwidth is nearly an order of magnitude greater than the temporal bandwidth of current pixelated modulators. A device with 500 (which is the number of channels needed to create a display with no vertical scanning) could provide enough bandwidth to drive a horizontal-parallax only (HPO) holographic display one meter in width (this is the demagnified length of the train of acoustic pixels generated by the device during 1/30th of a second--the duration of one frame). As of this writing I am fabricating devices with as many as 1250 channels.

The fabrication of active LC and MEMS devices requires as many as 20 or more mask steps to define filters, pixels and the associated backplane. Only two masks are required to fabricate guided-wave modulators: one to define the waveguide structure and one to pattern the transducers. The resulting fabrication and cost are similar to that of common SAW filters which sell for a dollar or less. A device capable of producing standard resolution HPO holographic video images would be in the low tens of dollars to fabricate as a conservative estimate.

Guided wave modulators are analog devices and can be driven by up-converted, standard analog video signals, generated by, e.g., standard graphics cards commonly employed in high-end graphics work. Since the modulators are analog and have no pre-defined pixel microstructure, there is no intrinsic quantization of the signal. The device transducers can be used as filters to band-limit quantization noise that might be present in the video signal. As with pixelated modulators, light may diffract from harmonics of the acoustic signal giving rise to higher-order diffracted signals; however, in anisotropic mode couplers typically only one order is present at the output of the device. This is because conjugate modes are prohibited by waveguide asymmetry and higher-order modes are distanced from desired output by high angular separation of low orders.

In addition to the points given above, three advantages of particular interest made possible by the waveguide nature of the device: hologram polarization rotation, increased angular deflection, and simultaneous and superimposed RGB modulation--are elaborated upon here:

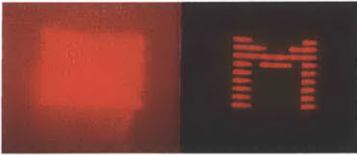


Figure 2-5 Polarization rotation

The scanned output of the modulator is shown without a polarizer (left) and with a polarizer to exclude noise (right)

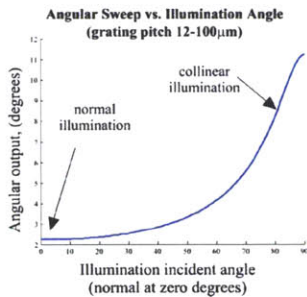


Figure 2-6 Angular deflection

Diffraction output angle vs. input illumination angle. This comes from the expression, $\text{Sweep} = \theta_2 - \theta_1$, where $\theta_1 = \text{asin}(\sin(\theta_{in}) - \lambda/\Lambda_1)$ and $\theta_2 = \text{asind}(\sin(\theta_{in}) - \lambda/\Lambda_2)$ given in degrees. Λ_1 and Λ_2 are 12 μm and 100 μm respectively and $\lambda = 532 \text{ nm}$.

1. POLARIZATION ROTATION

The waveguide in the guided-wave acousto-optic modulator is anisotropic so that it supports guided modes of only one polarization; modes of the orthogonal polarization are leaky. The acoustic signal couples light from the fundamental extraordinary guided mode to the first order leaky mode, rotating its polarization along the way [14], [15]. As a result, the holographic image produced by the anisotropic waveguide modulator has a polarization that is orthogonal to all of the other light in the system. This allows noise, including zero-order light, to be excluded from the output with a polarizer as shown in Figure 2-5.

2. WIDER ANGULAR DEFLECTION

Since the acoustic wave is being effectively illuminated by light at a glancing angle rather than at normal incidence, the resulting diffracted angle can be more than three times higher than it would be at normal incidence on another modulator of the same pixel pitch. This is shown in Figure 2-6 which was generated from the grating equation, shown left, where, θ_{in} , is the angle of the illumination light; θ_{out} , is the angle of the output light; Λ , is the grating period; λ , is the wavelength of light used and m is the diffracted order. Standard modulators are illuminated near the grating normal, but waveguided light interacts with the acoustic grating nearly collinearly. The differential effect of output angle with incident angle is shown in Figure 2-7. This effect is further magnified when the grating is inside a high index material as is the case in waveguide modulators. This is because the signal light is further deflected by refraction at the output face of the substrate. For the anisotropic modulator demonstrated in this paper, the output angle for 532nm light was measured to be 24.7 degrees for a 12 μm period acoustic grating generated on the device by a 326MHz RF signal. Since the anisotropic interaction limits the usable bandwidth of the modulator to approximately 50MHz [12] (per color) and because we use demagnification in our supporting optics to choose the final display view angle, only a fraction (2.6 degrees for 532nm light) of this angular extent is used. The modulator will present an output

that, when scanned, looks like a one meter image with a 2.6 degree viewzone. This image will be demagnified for a final display output with approximately 10 centimeters of extent and a 26 degree viewzone. Having a small input angle and a large demagnification ratio is intentional in my display as it reduces the requirements placed on the scanning optics and keeps the display compact. In my display geometry, the chief advantage of this angular expansion in anisotropic devices is that it gives approximately a five-fold increase in the rate of angular deflection (degrees of deflection per MHz of signal bandwidth) than is typically available to lithium niobate acousto-optic deflectors, bringing the angular rate of deflection of the anisotropic modulator to meet or exceed that of slow shear mode tellurium dioxide Bragg Cells but at a fraction of the cost and with the added advantages of lower acoustic attenuation and dramatically higher channel capacity.

3. SIMULTANEOUS SUPERIMPOSED RGB MODULATION

Anisotropic waveguide devices are capable of multiplexing color in frequency rather than in time or space. In LC, MEMS, and Bulk AO modulators, it is necessary either to dedicate pixels to one color or to illuminate sequentially the SLM thereby reducing the resolution or the maximum refresh rate.

However, waveguide devices can employ wavelength division multiplexing which allows for simultaneous and superimposed modulation of red, green, and blue light so no color filter wheel or separation of red, green, and blue channels is necessary. This effect arises because the phase matching condition is wavelength dependent. Red light mode converts at a lower frequency than green light which in turn couples at a lower frequency than blue, allowing one to choose which color to modulate by 'coloring' the frequency spectrum of the electrical signal sent to the modulator's transducers (see Figure 2-8). Because each channel is essentially a white-light emitter the illumination of the device becomes trivial. Each channel or group of channels can be flood illuminated by continuous red, green, and blue light sources.

This interaction is particularly well suited for color holographic displays because the phenomenon of leaky mode coupling allows enough bandwidth for each color to scan out a useful fan of angles but at the same time each passband is sufficiently separated to allow for independent operation. Furthermore, it is very convenient that all three color bands fit approximately within the 200 MHz available from analog video outputs of standard graphics processors.

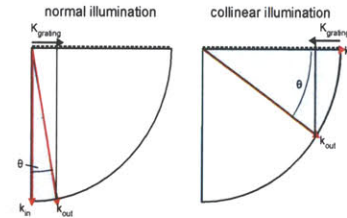


Figure 2-8 Collinear vs. normal illumination

Note that the angle of deflection is greater for collinear illumination than it is for normal illumination even though $k_{grating}$ is the same in both cases.

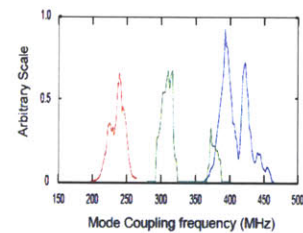


Figure 2-7 Frequency multiplexing of color

The waveguide modulator outcouples red at low input signal frequencies, green at middle frequencies and blue at high frequencies.

ANALOG VS. DIGITAL GEOMETRIES

Given the advantages of guided wave modulators, a new family of flexible holographic video displays is now possible. In holographic video displays using anisotropic mode couplers, the output of the device is scanned to create large outputs by persistence of vision. Since the modulator is an analog device, display parameters such as frame rate, view angle, image extent and vertical resolution can be interchanged fluidly as long as the bandwidth budget is satisfied. If more space-bandwidth product (which is related to the concept of numerical aperture and to the total number of scannable points in diffracting systems) is needed, the length of the channels can be extended to provide longer interaction lengths in accordance with the expression, $N = L(\Delta f)$, where N is the space-bandwidth product (or number of scannable points), L is the channel length, v is the velocity of the acoustic wave and, Δf is the bandwidth of the anisotropic mode coupling interaction. If more temporal bandwidth is needed, more channels can be added to the modulator. When there are enough channels in an array to write all the necessary output lines simultaneously, there is no longer a need for vertical scanning and the problem of holographic video display becomes reduced to a single axis scan. With all lines written at once, the scanning optics are only required to make a full sweep once every 1/30 or 1/60 of a second, greatly expanding the size and type of scanning elements that may be used, which, interestingly, means that large displays can be more physically parsimonious than small ones.

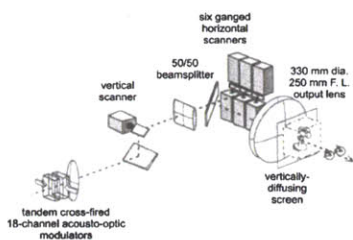


Figure 2-9 MIT Mark I Holographic video display

This display uses a telescope and a scanning polygon mirror to demagnify and descand the pattern on an acousto-optic modulator.

HOLOVIDEO MONITOR

The capstone of this dissertation work is the creation of the world's first low-cost, PC-driven holographic video monitor. There have been many holovideo displays created to date, many of them extremely impressive, but each of them has had one or more rather damning drawbacks when considered for use as a practical display technology which have made them more of a high-end science experiment rather than a tool for the masses. In this work we describe the creation of a display that has most of the attributes of a modest computer monitor: DVI inputs, postcard sized display output, 24-30 degree viewangle, standard video resolution, color operation and a bill of materials in the hundreds of dollars.

PREVIOUS GEOMETRY WORK

The geometry for my display is similar to that of the first MIT holovideo prototype Mark I[21], with a few differences. The Mark I

B A C K G R O U N D

and those geometries that preceded it were basically telescopes with polygons at the Fourier plane to scan (or more correctly, descan) the output of an AOM (see Figure 2-9). The same would be true in this geometry but the angles are larger and accordingly the output lens faster, so that the polygon can be smaller. The output lens will be reflective rather than refractive so that a larger numerical aperture might be obtained. Finally, the driving AOM in the system will be a multichannel guided wave modulator, and not a bulk-wave acousto-optic modulator. For early architectures based on modulators with only a few channels, a vertical scanning will be used to build up to standard vertical video resolution.

OVERVIEW OF THE TEXT

This dissertation contains chapters on theory, which outlines basic principles of SAW devices and waveguides; design, which gives an enumeration of the design decisions made during the course of this work; fabrication, which gives step by step instructions on fabricating devices and holovideo geometries and a results chapter which reports the results of device testing and characterization as well as demonstrating the final output of the holovideo monitor prototypes.

SUMMARY

In summary, all holovideo displays are based on spatial light modulators, typically pixelated modulators originally built for 2d displays which have been difficult to adapt to holovideo. We have introduced guided wave modulators, originally developed for telecom applications, as a solution for holographic video with a number of advantages over the previous state-of-the-art including lower cost, higher deflection angle and new capabilities such as polarization rotation and frequency division multiplexing of color. I have endeavored to use this technology to build the world's first low cost (<\$1000), PC-driven holographic video monitor.

B A C K G R O U N D

24

3

Theory

T H E O R Y

PIEZOELECTRIC MATERIALS

Piezoelectricity is the mechanical displacement that occurs in the presence of an electric field in non-centrosymmetric materials including quartz: lithium tantalate and lithium niobate,¹ all of which are useful as surface acoustic wave substrates.

Lithium niobate(LiNbO₃) is a synthetic ceramic belonging to the 3m point group. In addition to being a good piezoelectric material it has good transmission in the visible region of the electromagnetic spectrum and lends itself readily to the formation of surface waveguides by proton exchange and titanium in-diffusion.



Hooke's Law

Being piezoelectric, lithium niobate distorts (strains) when in an electric field. This deformation is subject to Hooke's Law which is given in tensor form as [16] (Xu page 28):

$$T_{ij} = c_{ijk} l_s$$

Where T is the stress induced by the electric field, S is the strain and c is the intrinsic elastic stiffness coefficient of the material. For a periodic excitation an acoustic wave is generated which is governed by the following coupled mode equations[12] (as given by Matteo et al.)

Coupled Mode Equations (acoustic)

$$c_{ijkl} \frac{\partial^2 u_k}{\partial x_i \partial x_l} + e_{kij} \frac{\partial^2 \phi}{\partial x_i \partial x_k} = \rho \frac{\partial^2 u_j}{\partial t^2} d$$
$$e_{ikl} \frac{\partial^2 u_k}{\partial x_i \partial x_l} - \epsilon_{ik} \frac{\partial^2 \phi}{\partial x_i \partial x_k} = 0 \dots i, j, k, l = 1, 2, 3$$

1 Bone collagen is a piezoelectric!

The wave solution is a Rayleigh wave with transverse and longitudinal components and a wave speed given by:

$$v = \sqrt{\frac{c}{\rho}}$$

(subscripts omitted) (Xu page 183) where, c , is the elastic stiffness coefficient for the waves in the direction of travel and ρ is the material density. The wave speed will be higher for metalized surfaces than for electrically free surfaces. Proton exchange and other waveguide formation techniques will modify the material stiffness and generally reduce the acoustic wave speed.

INTERDIGITAL TRANSDUCERS

The simplest form of interdigital transducer is formed by a uniform set of periodic electrode finger pairs. The fundamental characteristic of an interdigital transducer is its period. The period, along with the SAW wave speed determines the frequency of the excited wave through the equation:

$$f = v\Lambda$$

where, Λ , is the period, v , is the velocity and, f , is the frequency. The bandwidth of the transducer is roughly equivalent to:

$$\Delta f \approx f_c / N$$

where, N , is the number of finger pairs and, f_c , is the center frequency of the transducer[27]. However an interdigital transducer may be made of series of electrode finger pairs, each with a slightly different period (chirped) in which case the total bandwidth of the transducer is roughly equivalent to:

$$\Delta f \approx v \left(\frac{1}{\Lambda_2} - \frac{1}{\Lambda_1} \right)$$

where, Λ_2 , is the smallest period and, Λ_1 , is the largest period[27].

SAW Velocity



Lord Rayleigh

SAW Frequency

SAW Bandwidth (uniform transducer)

SAW Bandwidth (chirped transducer)

TRANSDUCER AS A CIRCUIT

Electrically, the interdigital transducer is both a capacitor (with lithium niobate as the dielectric) and an end-fire phased array antenna. The radiation resistance of the antenna is directly related to the energy of the launched SAW. The narrow fingers also create ohmic resistance. Smith [17] gives an equivalent circuit model for the interdigital transducer which takes these elements into account and facilitates the design of transducer impedances and impedance matching networks.

TRANSDUCER AS A WAVEGUIDE

The wave speed of acoustic propagation varies as a function of metalization of the lithium niobate surface. An interdigital transducer with regions of full and partial metalization will form an acoustic waveguide. The waveguide parameters will be especially important to consider for interdigital transducers with very large periods and small finger lengths which would lead considerable coupling to leaky acoustic modes--which requires a special method of coupled mode analysis[18].

TRANSDUCER AS A BRAGG MIRROR

The frequency response of a uniform transducer takes the form of a sinc in frequency. As waves propagate within the transducer, reflections occur which reinforce each other in the same way that a Bragg mirror's reflections reinforce constructively. The result is the formation of a 'stop band' in the center of the transducer frequency response. The influence of the stop band is to reduce the frequency response. The amount of reduction is dependent on the number of fingers, a design decision, and the magnitude of the reflection at each electrode which is tied to fundamental material properties. Electrodes on lithium niobate tend to reflect a lot relative to quartz and other SAW materials and stop band effects can be considerable for devices with a large number of uniform finger pairs.

Stop-band

The slowness of an acoustic system can be visualized with a slowness plot. The power flow angle can be determined as the normal to the slowness curve (Xu page 29). The powerflow angle may prevent the surface acoustic waves from traveling straight (nor-

mal to the transducer fingers) when launched from an interdigital transducer.

WAVEGUIDES

In free-space, Maxwell's equations give us plane wave solutions which travel at the free-space (phase velocity) of light in the surrounding medium. However, once free-space is quantized by waveguide boundaries then the solutions of Maxwell's equations must satisfy boundary conditions. Intuitively, we can arrive at the new solution by imagining a ray bouncing back and forth between the boundaries of a waveguide. This ray can be thought of as being composed of three different components: a component going up, a component going down and a component traveling directly along the waveguide. The up and down components combine to form a standing wave pattern that becomes the guided 'mode shape' which satisfies the boundary conditions. These conditions require continuous amplitude and slope of the E field across the boundary. These conditions can also be equivalently expressed as matching amplitude of both the E and H fields across the boundary. The remaining component moves with a speed that is slower than the phase velocity of light. This is simply because light moving in zig-zags gets from a to b more slowly than light traveling in a straight line. The effective speed of the guided light is the group velocity². This effective velocity gives rise to an effective index of refraction that lies somewhere between the index of the waveguide and the index of the cladding. When the effective index of the guided-wave drops below the effective index of the cladding, the light is no longer confined and begins to escape as a leaky mode. Thanks, in large part, to the continuity of fields across boundaries, a guided mode can be largely characterized by its effective index, or more commonly, a related quantity, its spatial frequency, often called 'Beta' or the 'wavenumber'. This is just a quantity describing how much of the guided light's momentum is moving down the waveguide and not stuck bouncing up and down between the waveguide boundaries. Furthermore, we can use the wavenumber in momentum

² It is this concept of group velocity that has given rise to the somewhat misleading term, 'slow light', in resonant optical structures.

diagrams and K-plots to more intuitively describe what is going on inside waveguide systems (see Figure).

CONJUGATE MODES

Waveguide asymmetry performs a practical purpose in this system. The air/guide interface has higher index contrast than the guide/substrate interface and so it continues to act as a perfect mirror even for modes that have leaked into the substrate. For SAW patterns that diffract light into holographic images, this means that there is no diffracted, or mode coupled, conjugate light (no evil twin). There are other higher order modes that are polarized with the output light but they are separated from the mode of interest by large angles.

MODE COUPLING

In birefringent material TE light may see a waveguide when TM light does not. In such a system, if we were able to change the TE guided light into TM light in the waveguide, then the resulting light would no longer be guided and would leak into the substrate. This is the fundamental phenomenon behind the operation of the devices described in this research, i.e., mode-coupling from guided to leaky modes. For this to occur, we must have three things:

1. A break in symmetry (provided by the crystalline material)
2. Overlap of TE and TM mode shapes.
3. Phase matching between TE and TM modes.

ASYMMETRY

(give point group images)

The asymmetric nature of the lithium niobate crystal structures provides the asymmetry we need to convert light from one polarization to another. Additionally the crystal structure dictates which cuts and propagation directions will allow mode-coupling.

OVERLAP AND COUPLING COEFFICIENTS

The coupled mode equations that govern the transfer of light from

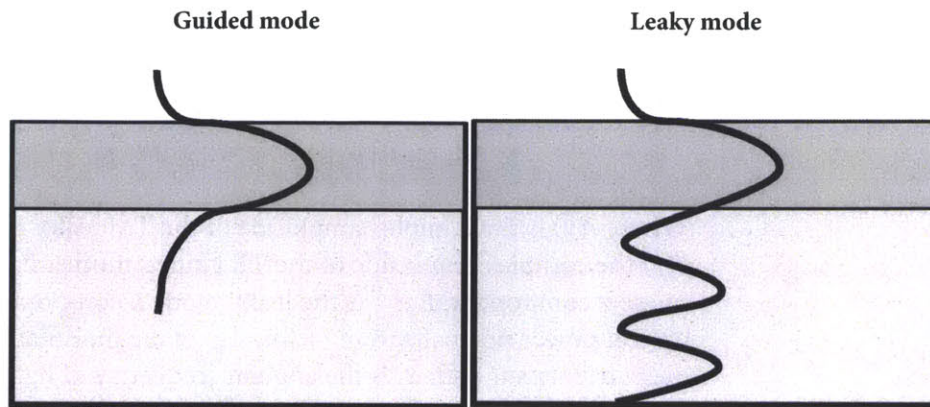


Figure 3-1 Waveguide modes

(left) An index guided mode is evanescent in both the air and substrate. (right) A leaky mode is evanescent in the air but has a propagating component in the substrate. The mode can be gap guided or index guided. In single color devices only shallow waveguides are used that possess one or two modes. For multi-color devices, deeper waveguides which support three or more modes are employed. In all cases only one or two guided modes are used as the input modes (usually the fundamental) and the other guided modes are ignored.

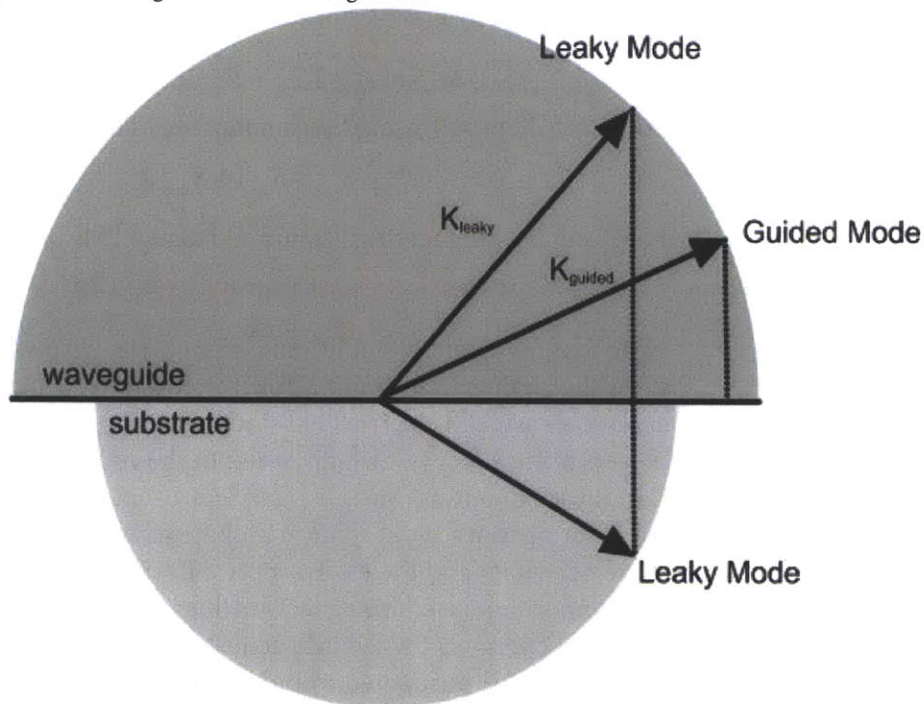


Figure 3-2 K-space view of waveguide modes

It can be helpful to visualize waveguides modes with a k-space diagram. Here the large semicircle has a larger radius corresponding to the larger momentum vector of light travelling in the material. For rays traveling below critical angle, the projection of the momentum vector will lie inside the waveguide semicircle where it is guided and outside the substrate circle where it is evanescent. The projection of a leaky mode would be inside both semicircles.

one mode to another are given here[19] (from Marcuse)

**Coupled Mode Equations
(optical)**

$$dg(y) / dy = -i\beta_{gm}g(y) - i \int K_{gr}r(y) d\beta_r$$

$$dr(y) / dy = iK_{gr}^*g(y) - i\beta_r r(y)$$

$$K_{gr} = (\omega / 4P) \int \Delta\epsilon_{zx} E_z^{(TE)*} E_x^{(TM)} dx$$

**Dielectric Tensors for Leaky
Mode Coupling**

Where $r(y)$ is the complex amplitude of the TM leaky mode and $g(y)$ the complex amplitude of the TE guided mode. $E_z^{(TE)}$ is guided mode z component, $E_x^{(TM)}$ is the leaky mode x component. P is the optical power normalization factor, $\Delta\epsilon_{zx}$ is the modulation of the dielectric tensor and, ω , is the angular frequency of light. K_{gr} is the TE-TM coupling coefficient. The mode-coupling coefficient, K_{gr} , is dependent on the overlap of the mode shapes as well as a modulation term. The modulation term will vary based on the crystal cut and acoustic wave propagation. Only three orientations/propagation directions give rise to polarization-rotating wave coupling[15]:

For X-cut Y-propagating lithium niobate (TE-TM coupling)³:

$$\Delta\epsilon_{zx} = P_{yzyz} 2S_{zx} + P_{yzxx} 2S_{xy} + r_{zxx} E_x$$

For Y-cut, X-propagating lithium niobate (TE-TM coupling):

$$\Delta\epsilon_{zx} = P_{yzyz} (S_{xx} - S_{yy}) + S_{yzyz} 2S_{yz} + r_{zxx} E_y$$

For Z-cut, X-propagating lithium niobate (TM-TE coupling):

$$\Delta = P_{yzxx} (S_{xx} - S_{yy}) + S_{yzyz} 2S_{yz}$$

Note that for Y and X-cut lithium niobate the permittivity (which gives the change in index of refraction induced by the surface acoustic wave and electric field) includes contributions from the piezoelectric effect (which gives rise to the strain, S and the field E in these equations) and also the electro-optic effect (shown as r). Not only does Y-cut lithium niobate have contributions from piezoelectricity and the electro-optic effect it also has the largest electromechanical coupling factor (this is the efficiency with which electrical energy is turned into acoustic energy using a transducer) which ITO[15] postulated would have an effect (Y-cut electro-mechanical coupling factor (K^2) is approximately .05. For X-cut

³ I made an effort to dig up these tensor values and I give them with the warning that they should be checked before being used:

$P_{yzyz}=0.146[31]$, $P_{yzxx}=-0.151[31]$, $r_{zxx}=10.5 (10^{-12}m/V)[30]$

it is .035 and for Z-cut .0052 (from slobodnick)⁴. It would seem natural to use Y-cut lithium niobate, however the standard proton exchange techniques (benzoic acid immersion) damages the surface of Y-cut lithium niobate[20]. This can be mitigated with titanium indiffusion, but for simplicity we use X-cut lithium niobate which has higher electromechanical coupling than Z-cut and is undamaged by proton exchange.

PHASE MATCHING

In mode-coupling, an acoustic phonon of particular momentum is 'knocking' light from a TE mode to a TM mode. For this to occur momentum must be conserved along the propagation direction. Momentum need not be conserved in the axis that runs through the waveguide because there is no symmetry in this direction, instead, conservation of momentum is required only along the waveguide which has continuous translational symmetry. This follows from as a mathematical result found by Emmy Noether.

The phase matching condition is shown below:

$$\vec{\beta}_{guided} - \vec{K}_{acoustic} = \vec{\beta}_{leaky}$$

The wavenumber (also the momentum) of the TE mode minus the wavenumber of the TM mode is equal to the momentum of the surface acoustic wave. K_a is equivalent to $2\pi/\Lambda$ where Λ is the period of the acoustic wave.

FREQUENCY RESPONSE

Guided modes only allow the propagation of discrete spatial frequencies. This is because guided modes have standing wave components that live in the high Q resonator created by the boundaries of the waveguide. If any light in the waveguide were to deviate even slightly in spatial frequency it would eventually destructively interfere with itself as it bounced back and forth, infinitely, in the waveguide.

Leaky modes, however, do not bounce back and forth infinitely. Gradually all the power leaks out of the guide which results in a lossy, low Q resonator which is more tolerant of variation in spa-



Emmy Noether

Phase-Matching Condition

⁴ Try not to confuse K_{gr} the coupling efficiency of energy from TE light to TM light with K^2 the coupling efficiency of electrical energy to acoustic energy.

tial frequency--though not so much as free-space which allows all spatial frequencies (because there is quantization, no waveguide no resonator and no Q). So it is possible to couple light from a guided mode to a leaky mode over a range of spatial frequencies.

The depth of the waveguide has an effect on the mode-coupling frequency and bandwidth with deeper guides having smaller mode-coupling frequencies and bandwidths⁵. This is because, as waveguides get deeper, they admit more modes, which become more closely spaced in spatial frequency. Also, increasing depth shifts the center frequency of the mode-coupling response.

In multicolor systems these dependencies mean red, which sees a shallow guide relative to its wavelength, couples at lower frequencies and with higher bandwidths than does green or blue, which see shallower guides and narrower bandwidths. The shifting of the center frequency with wavelength is the basis for frequency division multiplexing of color for diffractive displays which is one of the more novel contributions of this dissertation work.

THE GRATING EQUATION

Momentum arguments, similar to the one above, gives rise to what is perhaps the most useful and general equation in holography: the grating equation,

$$\sin \theta_{out} - \sin \theta_{in} = m \frac{\lambda}{\Lambda}$$

Where, θ_{in} , is the input angle, θ_{out} , is the output angle, m is the diffracted order, λ , is the optical wavelength and, Λ , is the grating period.

The equation tells us how much light will deflect off of a grating (including acoustic gratings) of a given period. Note that the equation is not linear. It is hyperbolic. This means it is very linear for coarse gratings illuminated perpendicularly, but nonlinear when the grat-

⁵ Note that, for mode-coupling frequency, waveguide depth is a secondary factor. The most sensitive dependence for mode-coupling frequency is the birefringence of the waveguide.

ing is illuminated from the glancing, or nearly collinear angles. In the nonlinear, collinear regime, light is deflected over much higher angles as the grating period increases. This means that waveguide mode-coupling modulators can deflect light over much larger angles than normally illuminated spatial light modulators.

GEOMETRY

The geometry of the holographic video display described in this dissertation is a confocal telescope with a scanning mirror at the focal plane. It is based largely on the MIT Mark I holographic video prototype [21] and is subject to the same mathematical description though it is somewhat less constrained by bandwidth considerations.

Magnification

DEMAGNIFICATION

The transverse magnification for the confocal geometry (from St-Hilare pg 27):

$$M_t = -\left(\frac{f_2}{f_1}\right)$$

And longitudinal magnification:

$$M_l = M_t^2 = \left(\frac{f_2}{f_1}\right)^2$$

DEROTATION

The surface acoustic wave is made to appear stationary by observing its motion in a spinning polygon mirror.

POLYGON SIZE

The Mark I polygon was a fearsome thing to behold. It had a diameter greater than 10cm, more than a dozen facets and would spin so fast that witnesses described looking into the display as being akin to placing your face three inches from a circular saw. At the end of his dissertation Dr. St-Hilare gives several suggestions for improvements which were implemented in my dissertation work. He suggests at the end of his dissertation that a higher bandwidth crystalline material and this requirement was satisfied with my

Holovideo Image Size

choice of lithium niobate and my development of SAW rather than bulk mode modulators for holovideo. He has also suggested using reflective optics for the output lens with lower f-numbers to keep the display compact and inexpensive. This suggestion has also been followed and I would note that having a low f-number output lens reduces the necessary size of the polygon facets through Dr. St-Hilare's equation for the Fourier plane size:

$$dx = d \sin\left(\frac{\theta}{2\Omega}\right)$$

where, dx , is image size, θ , view zone and, Ω , is polygon scan angle.

We have been able to reduce the facet size by suppressing the Ω term, by having fewer facets on the polygon and then using a faster lens to catch the more rapidly diverging output of the scanning optic. This means a smaller number of lines per second, but a smaller polygon can go faster to make up the deficit without the threat of a large scary metallic death object in the display. Furthermore, because our devices can be made to have as many channels as there are vertical lines in the display, large displays can be made with large, slow moving polygons that may be required to rotate no more than once or twice as second. (In fact, such a polygon would have to become the time keeper in display because locking such a slow polygon would prove very difficult). A further advantage of this large instantiation would be that it would not need any vertical scanning as every vertical line is written simultaneously, making large displays more mechanically parsimonious than small ones.

T H E O R Y

37

T H E O R Y

38

4

Design

D E S I G N

The design of the waveguide modulator, and the display that supports it, required hundreds of decisions, from which of the dozens of methods of proton exchange to use to form waveguides to what frame rate should be chosen in the final display. Often these decisions were based on the results of careful experimentation and mathematical analysis but sometimes I chose design parameters entirely because they were the most common in the literature and for no other reason. On a few rare occasions, I was left to just make my best guess. This chapter attempts to explain the rationale behind my most important design decisions as well as pointing to other possible paths of exploration for those seeking to continue this research.

WAVEGUIDE INTRODUCTION

The waveguide device is the marriage of integrated optics and surface acoustic wave devices, and as such, inherits all the tools and techniques available to both of these mature fields. The enormity of the choices available is a blessing and a curse. On one hand, finding an optimum set of parameters requires a large amount of testing and exploration, but on the other hand, I have the consolation of knowing I have many degrees of freedom to help me overcome any design challenges that may arise.

For the most part, my approach has been to pick design points that have been reported to work well in the literature and then to explore the design space near and between these points. In particular, I was heavily influenced by Ito [15] and Rust [13].

DECISION TREE

A graphic illustrating the design choices made in creating the waveguide modulator is shown right.

SUBSTRATE MATERIAL

The first choice to be made for my device was that of the crystalline piezoelectric substrate. Any material commonly used for surface acoustic wave devices was a potential candidate: lithium niobate,

Waveguide Modulator Decision Path

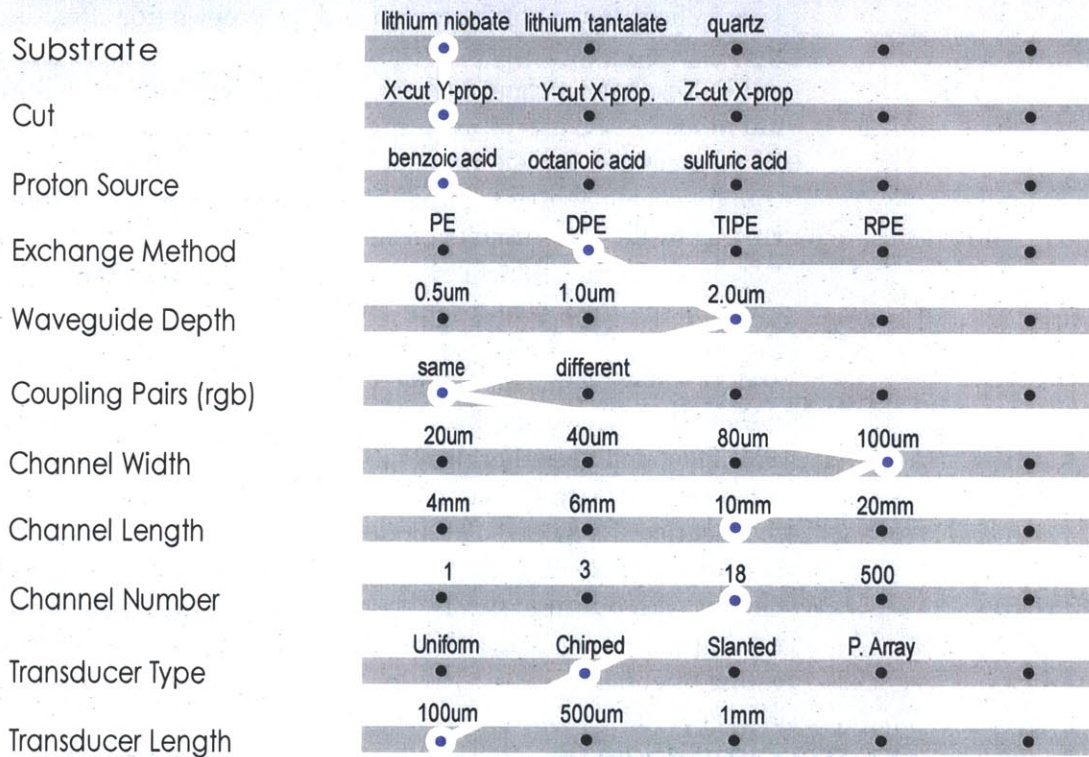


Figure 4-1 Waveguide modulator decision tree.

This chart summarizes many of the decisions I had to make during the design of my waveguide modulators.

lithium tantalate or quartz. Lithium niobate has the highest electromechanical coupling coefficient but poor temperature stability. Quartz has the best temperature stability but low efficiency. Lithium tantalate lies somewhere in between on both counts. Because optical diffraction efficiency is of the utmost importance in my devices, and because optical diffraction efficiency is closely tied to electromechanical coupling efficiency, I chose lithium niobate as my device substrate.

MATERIAL CUT AND ORIENTATION

Next I chose the cut of the crystal and the propagation direction of the surface acoustic waves. Polarization rotating mode coupling is only allowed for certain cuts and propagation directions in lithium niobate: X-cut Y-propagating, Y-cut X-propagating and Z-cut X-propagating. Y-cut wafers have the highest electromechanical coupling coefficient of the three cuts but its surface is vulnerable to etching by the acids used to create waveguides in lithium niobate. I could solve this problem by pre-treating the Y-cut surface with titanium indiffusion which prevents etching but adds complexity to the processing. I decided to abandon Y-cut for this iteration and to make a note to come back and try it at some future date. Z-cut has the smallest electro-mechanical coupling coefficient but it supports TM-TE coupling (rather than TE-TM coupling as is the case for the other two cuts) which is interesting for several reasons including the fact that the guided TM mode sees the same index of refraction in all directions which might be useful if I wanted to integrate other devices with our modulators (such as Bragg Deflectors) but I was not implementing Bragg deflection so I selected a X-cut Y-propagating orientation.

PROTON SOURCE

There are a number of acids that might be used as proton sources to create waveguides in my substrate including: benzoic acid, octanoic acid and sulfuric acid. Benzoic acid is, by far, the most commonly used acid for proton exchange and has and has been well documented in the literature. Benzoic acid has the highest proton exchange rate of the three candidates. One disadvantage of benzoic acid is that it is solid at room temperature which can make

it difficult to work with as your device samples are encased in a solid after the acid bath temperature falls under 150°C. Octanoic acid has been presented as a safer alternative to benzoic acid [22] (though benzoic acid crystals have low toxicity)¹. Octanoic acid has a slightly lower exchange rate but has the advantage that it is liquid at room temperature. Sulfuric acid is ubiquitous in cleanrooms but is fairly dangerous. Heated sulfuric acid is unpleasant to contemplate so I dismissed that option. Octanoic acid is tempting but the fact that Benzoic acid has been so thoroughly explored made it the best choice for predictable results.

EXCHANGE METHOD

The waveguide is formed by some combination of pre-treatment such as titanium indiffusion, followed by proton exchange in pure, dilute or vapor phase acid melt, and finally, a post treatment which typically consists of annealing in air or some inert gas or in a salt melt to reverse the proton exchange process and bury the waveguide [23]. Titanium indiffusion as a pre-treatment step is helpful for preventing etching on Y-cut substrates and for creating waveguides with tunable birefringence. Pure melts of benzoic acid usually give lossy waveguides with poor electromechanical properties. Dilute melts and vapor melts create better quality waveguides, though too much dilution can make the waveguide vulnerable to optical damage [24]. Often in the literature for X-cut devices, waveguides are made by proton-exchange in a melt of benzoic acid diluted with lithium benzoate (which accounts for 1% of the final melt mixture by weight) and then by annealing the guide at 375°C for 45 minutes. This is the combination of steps that I chose to use in my devices, though I may investigate reverse proton exchange later to see if it improves the device performance.

WAVEGUIDE DEPTH

The waveguide depth determines the number of modes supported by the waveguide. Ito reported the highest diffraction efficiency for devices made with relatively shallow guides [15]~0.5um but I have

¹ In fact, benzoic acid occurs naturally in berries and is used as a food preservative.

observed that deeper guides tend to have lower loss. In particular there seems to be a jump in waveguide quality when a waveguide becomes deep enough to support a second mode (at a depth of approximately 1 μ m). High diffraction efficiency is important for achieving sufficient display brightness and for keeping the displays power requirements reasonable, however, the lower the loss of the waveguide the longer the interaction lengths can be and the more the number of discernible views in the output of the display. Taking all these considerations into account, I elected to try both a shallow single mode and a deeper, two-mode waveguide and compare the outcome in my display.

COUPLING PAIRS

When more than one mode is present in the waveguide it is sometimes possible that transitions between higher modes are more efficient than those of lower modes. This may have something to do with the degradation of the material properties within the waveguide after proton exchange. This degradation within the waveguide may give an advantage to modes with a lot of optical energy outside the waveguide in evanescent fields as is the case with higher order modes, as was suggested by Rust and Strake [13]. This is unlikely to be an option for red light which will have only one or two orders for the waveguide depths I chose, but green and blue light will likely have more modes and may present me with this additional option. Using higher orders for different colors create a lack of uniformity in the angular output spread of the device which can make recombining the outputs difficult in an RGB system. For this reason, I chose to forgo the potential increase in diffraction efficiency for green and blue and keep the transition modes the same for all three colors.

CHANNEL WIDTH

Waveguide channel width is an important parameters for diffraction efficiency in my devices. Waveguides created by proton exchange are convenient for acousto-optic interactions because they guide both optical and acoustic waves[25]. High diffraction efficiency can be achieved by creating narrow waveguide channels that create high optical and acoustic energy densities. The lower limit on channel width is determined by the acoustic wave cut-off frequency which is, in turn, determined by the acoustic velocity difference between the waveguide and the surrounding regions. The

velocity will vary depending on the cut, the proton exchange method and the annealing parameters. Rather than trying to predict this value, I decided to simply make a number of devices with varying channel widths and see which one provided the best diffraction efficiency with other parameters being equal. The best channel width, determined by my test, was a channel with a 100 micron 'mouth' tapering to a 80 micron minimum channel width. The fact that this waveguide had better output efficiency than the 100 micron/40 micron channel or the 100 micron/20 micron channel may have had more to do with the low ratio between the waveguide mouth and the minimum channel width than the overlap of the acoustic and optical wave, but I chose to go with this value anyway and made a note to perform another test with waveguides that possess the same rate of taper.

CHANNEL LENGTH

Channel length also strongly influences diffraction efficiency and provides a limit to the maximum interaction length and therefore the maximum number of views in the final display output. Theoretically, the maximum channel length is limited by the optical and acoustic loss in the waveguide. Practically, the maximum waveguide length is dictated by the thickness of the substrate. This is due to the leaky mode light entering the substrate from the waveguide at an angle of about 7-10 degrees from the substrate surface. After traveling through substrate, the light exits the edge of the wafer. If the interaction length is too long and/or the substrate is too thin, the leaky mode light will encounter the bottom surface of the substrate before reaching the edge of the wafer, effectively truncating the usable interaction length. As a rough estimate the maximum interaction length is five times the wafer thickness. I am using 3 mm wafers, so I could envision making channels as long as 15 mm, but because I would like to fit as many devices on a wafer as possible I chose to make the interaction lengths between 6 and 10mm.

CHANNEL NUMBER

The PC driving my display has 18 RF outputs which I will match directly to 18 channels on the device. Each channel in my device is driven by a signal with 200 MHz bandwidth for a total bandwidth of 3.6 GHz or 7.2 billion pixels per second.

TRANSDUCER TYPE

SAW transducers allow an enormous amount of variation, but most SAW transducers fall into one of three categories: uniform, chirped or slanted. Uniform transducers are the most straightforward to design and fabricate but the bandwidth and the efficiency of these transducers are tightly coupled. Chirped and slanted transducers break this coupling and allow for customized frequency response and adjustable efficiency. Of these two, chirped transducers are the easiest to design and fabricate so they were my transducers I chose to fabricate.

TRANSDUCER DIMENSIONS

The fundamental transducer dimension is the transducer period which determines the transducers frequency of operation. Since I have three different colors to consider, each of which will have a different operation frequency, my transducers will actually be a composite of three transducers designed to operate around the mode coupling frequencies for red, green and blue, respectively. If I desired, I could use the rate of chirp to modify the frequency response of the transducer to be as flat as possible within the band of mode coupling frequencies.

The width of the transducer is roughly matched to the width of the waveguide channel. The total length of the channel transducers is chosen to be some arbitrary length like 1.5 mm which is fast to write, but provides enough space to place a large number of fingers appropriately spaced with the periodicity determined above. I should note, that the larger the number of fingers the higher the internal reflections and the larger the effect of the acoustic stop band (acoustic Bragg reflection), however the chirping of the device is sufficiently large to diminish this effect.

ANGULAR SWEEP

The angular output sweep of the modulator is a function of the angle of the light traveling in the waveguide. The first order mode typically gets more and more collinear the deeper the waveguide becomes. For high angular deflection, we want deep waveguides and low order modes. This was previously determined for me by my choice of mode number and waveguide depth.

DESIGN SUMMARY

A summary of my waveguide design decisions is given in the figures below.

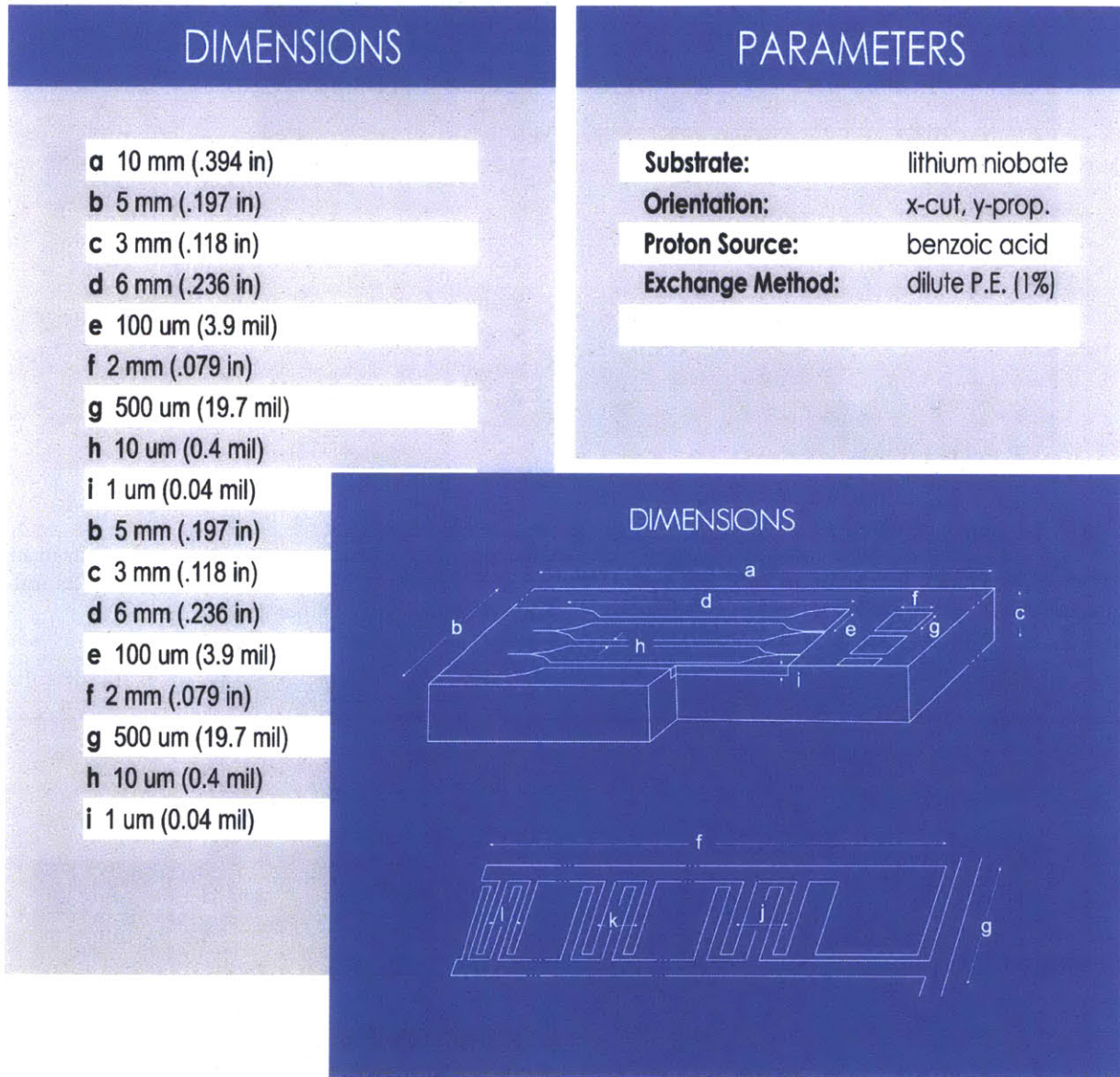


Figure 4-2 Design summary for waveguide device.

The tables and images above give the dimensions for the and the waveguide parameters for the typical device used in this dissertation work.

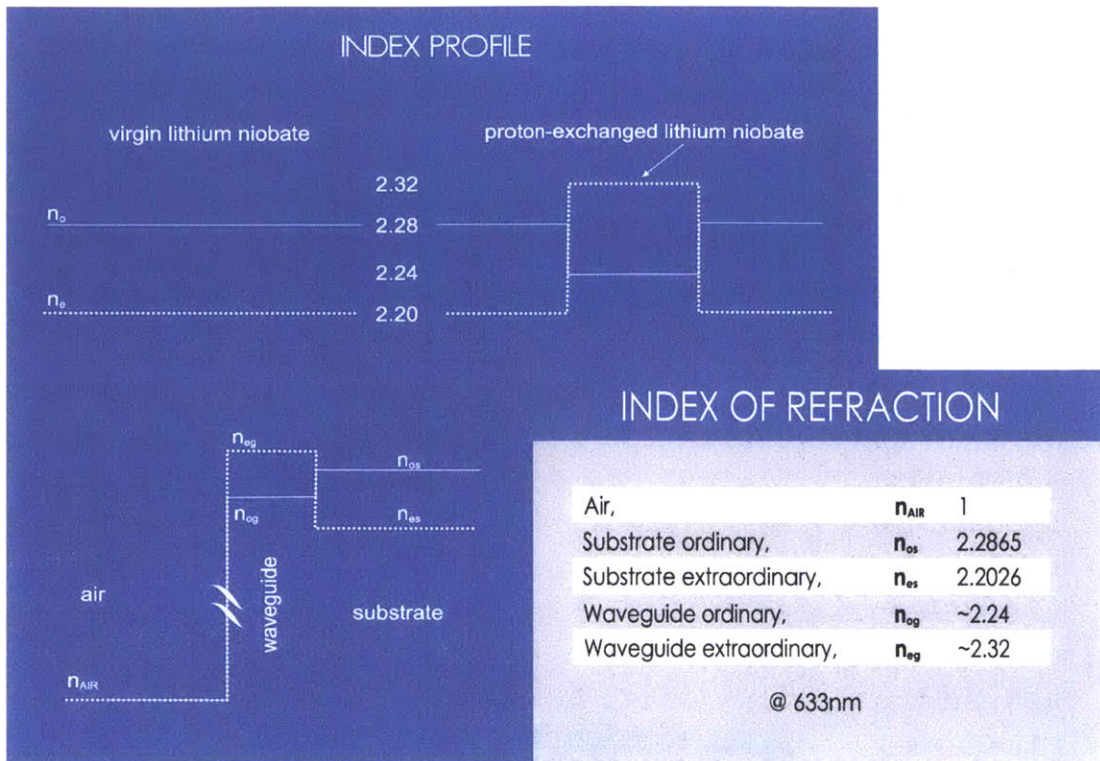


Figure 4-3 Index profile.

The index profile for a proton exchanged waveguide created in a pure melt of benzoic acid step-like and results in an extraordinary index increase of $\Delta n_e = 0.12$ and an ordinary index decrease of $\Delta n_o = -0.4$ [11]. Dilute melts and annealing will soften this profile but for this should be a good first order approximation for our design.

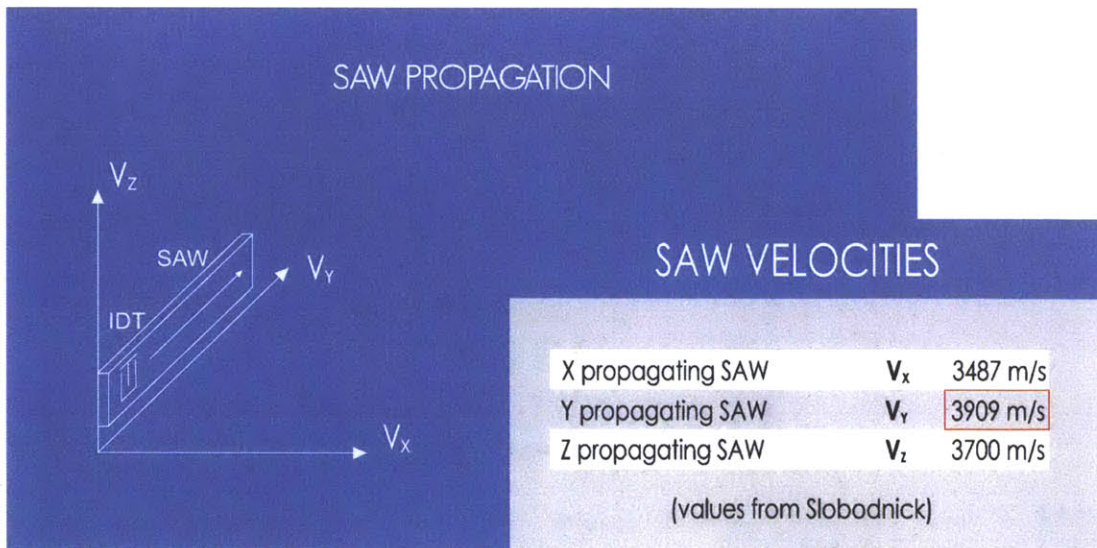


Figure 4-4 SAW Velocities.

The devices used in this work are primarily X-cut devices with surface acoustic waves propagating along the Y direction. Slobodnick et al.[27] has given detailed tables of velocities for each of these cuts. These proton exchange will change these velocities somewhat[12] but they serve as a good first order estimate.

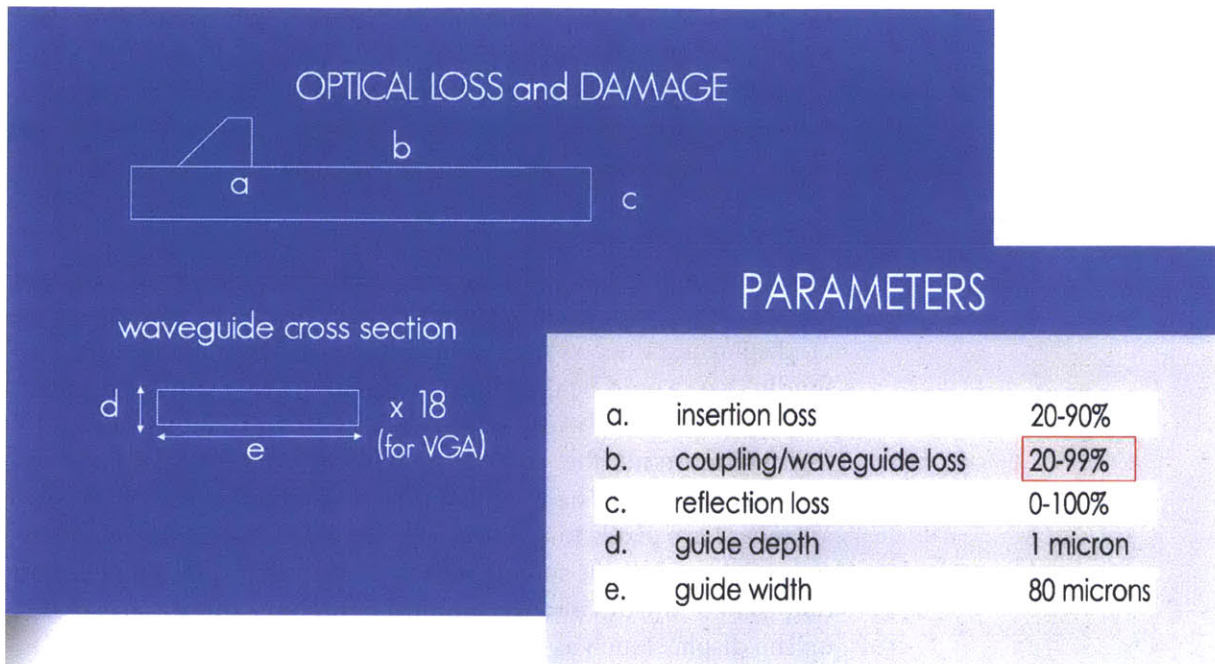


Figure 4-5 SAW Velocities.

The devices used in this work are primarily X-cut devices with surface acoustic waves propagating along the Y direction. Slobodnick et al.[27] has given detailed tables of velocities for each of these cuts. These proton exchange will change these velocities somewhat[12] but they serve as a good first order estimate.

Power Density Calculation

- 1) Assume 50% input loss, 10% efficiency and no reflection at output
- 2) CRT and LCD brightness is approximately 100cd

Convert cd to mW/steradian(sr)	$100\text{cd} = 146\text{mW/sr}$
Calculate total illumination	$146\text{mW}/0.1 = 1.46\text{W}$
Calculate per channel power	$1.46\text{W}/18 \text{ channels} \approx 81\text{mW/channel}$
Calculate power density	$\frac{81\text{mW/channel}}{80\mu\text{m}^2/\text{channel}} \approx 1\text{mW}/\mu\text{m}^2$

Figure 4-6 Optical power density.

We calculate a power density of $1\text{mW}/\mu\text{m}^2$ as a power density for an 18 channel device (the number of channels, minimum, needed for a VGA resolution display) with channels $80\mu\text{m}$ wide. This density is well above the optical damage threshold for visible light in virgin lithium niobate which is on the order of microwatts per square micron but not necessarily above the threshold for certain types of proton exchanged lithium niobate, like reverse proton exchanged lithium niobate (RPE), which may have a damage threshold above this density for visible light (532nm) in the milliwatts per square micron[29]. Keep in mind that additional channels can easily be added to dilute the power density to a tenth of this calculated density or more to give added headroom if needed.

GEOMETRY INTRODUCTION

I want to build a holographic video monitor. In particular I want to create a computer peripheral that has, as nearly as possible, the affordances of a standard video monitor including: standard video resolution (approaching 480 vertical lines), 30Hz refresh rate, and full color. These choices constrain the display viewzone and extent according to the bandwidth budget relationship.

BANDWIDTH BUDGET

The holographic video display described in this dissertation is an analog device which, among other things, means that we can trade off display parameters such as device size and frame rate more fluidly than would be possible in a digital display within the constraints of the 'bandwidth budget'. The bandwidth budget refers to the maximum number of pixels provided by the spatial light modulator per second. The modulator has no pixel structure so we can arrange these pixels to a wide variety of image aspect ratios, frame rates and resolutions so long as they do not exceed the total temporal pixel bandwidth and the physical limitations of the parts making up the display (such as the scanning optics).

I have 18 channels with a bandwidth of 50MHz each (for an RGB system) for a total of 900MHz which is equivalent to a maximum pixel frequency of 1.8 billion pixels per second. Within this budget we can build a wide range of displays.

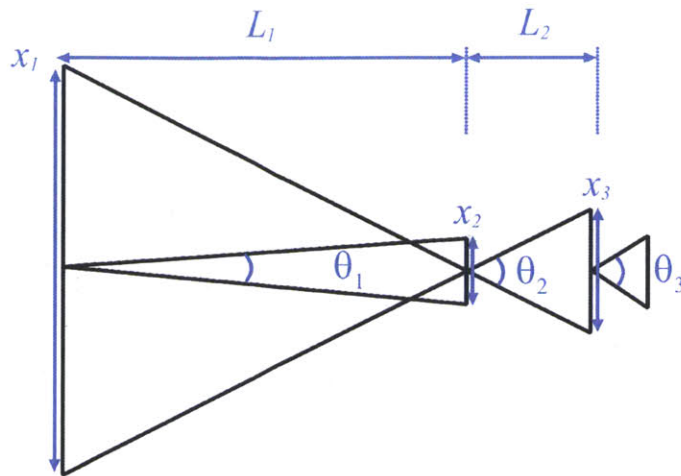
DESIGN STEPS

The steps for designing a holographic video display geometry are given, in order, on the facing page.

Figure 4-7 Display design steps (facing page)

The optical geometry of my holovideo monitor can be simplified to a set of angles, apertures and focal distances. The first aperture, x_1 , is the scanned aperture of the spatial light modulator which can be several meters. The actual aperture of the modulator makes up only a small fraction of this distance, 1-3 millimeters. The maximum angular diffraction sweep from the modulator is θ_1 . The aperture, x_2 , is the aperture imposed by the polygon facet size, typically 1-10 centimeters. The polygon scan angle which varies as a function of the number of polygon facets ($720\text{deg}/N$) is given as, θ_2 . The output image size is x_3 and the output view angle, θ_3 . The first and second focal distances, f_1 and f_2 , are the focal lengths of the transform lens and the output parabolic reflector, respectively.

The equations for these parameters are given in an order that makes sense for a holovideo display designer with the tightest constraints, such as polygon size, being established first. These equations assume that the modulator output sweep angle is filling the polygon aperture.



DISPLAY DESIGN STEPS

ORDER OF OPERATIONS

- 1) Choose polygon facet size, x_2
- 2) Choose the target output view angle, θ_3
- 3) Choose the modulator output angle, θ_1
 - Calculate first focal length $x_2 / (2 \tan(\theta_1 / 2)) = L_1$
 - Calculate demagnification ratio $\theta_3 / \theta_1 = D_{mag}$
 - Calculate second focal length $L_1 / D_{mag} = L_2$
- 4) Choose number of polygon sides, N_{poly}
 - Calculate polygon scan angle $720^\circ / N_{poly} = \theta_2$
 - Calculate scanned aperture $2L_1 \tan(\theta_2 / 2) = x_1$
 - Calculate output image size $x_1 / D_{mag} = x_3$
 - Calculate output lens f-number $x_3 / L_2 = f_{num}$
- 5) Choose polygon facet scan rate, v (facets/sec)
 - Calculate scan period $1/v = \tau$
- 6) Choose frames per second, fps
 - Calculate vertical resolution $v / fps = N_{res}$
- 7) Provide SAW velocity, V_{SAW} (for your choice of substrate)
 - Calculate oversampling $\tau V_{SAW} / x_1 = O$

POLYGON FACET SIZE

The first choice to be made is the choice of a polygon facet size. For inexpensive displays, this will not be a choice as only one size of inexpensive type of polygon is available (~20mm to 25mm for mass-produced polygons). However, for an expensive display with a custom polygon, this choice will be important as the maximum achievable display image size will depend more on the polygon facet size than on any other parameter. Reasonable polygon sizes will range from a 2cm to as much as 7cm. Large facet sizes lead to large expensive polygons.

DISPLAY VIEW ANGLE

Assuming that the display will be viewed from a distance of 0.5 meters the view angle should be chosen to be no less than 7 degrees. This is the minimum view angle that can still fit the pupils of a person with average interpupillary distance. Large view angles, e.g. above 45 degrees, require the display's output lens operate well outside the paraxial approximation which increases distortion. A 30 degree viewzone provides a modest amount of motion parallax and places reasonable requirements on the display optics.

MODULATOR SCAN ANGLE

The output angle of the spatial light modulator has historically been so small that there hasn't been much of choice of modulator angle. However, guided wave modulators fabricated for wide angular deflection allow for deflections from 0 to 8 degrees or more. For our design, we'll consider that we want each modulator to operate at 50Mhz bandwidth and then use whatever angular output that gives us (between 3 and 5 degrees typically).

FIRST FOCAL LENGTH

To determine the first focal length we just move the modulator away from the polygon until it's angular sweep fills the polygon facet. Mathematically, this is given as:

$$\frac{x_2}{2 \tan\left(\frac{\theta_1}{2}\right)} = L_1$$

DEMAGNIFICATION RATIO

From the modulator output scan angle and the target view angle we can determine the Demagnification ratio as:

$$\frac{\theta_3}{\theta_1} = D_{mag}$$

Lower ratios are easier to implement. Ratios of more than 20 are difficult to obtain in practice.

SECOND FOCAL LENGTH

The second focal length follows as:

$$\frac{L_1}{D_{mag}} = L_2$$

POLYGON FACET NUMBER

After the polygon facet size, the facet be the next most important factor to determining the final display size. This is because the polygon lies at the Fourier plane and high angle in this plane translates to large image extent through the Fourier transform.

The choice of polygon facet number will also determine the total size of the polygon which becomes large rapidly with additional facets for low facet numbers. Low facet numbers and large facet sizes also lead to polygons which act as “air pumps” with the edges of the facet beating the air and making the polygon noisy.

POLYGON SCAN ANGLE

The scan angle of the polygon is determined as follows:

$$\frac{720^\circ}{N_{poly}} = \theta_2$$

TOTAL SCANNED APERTURE

The physical aperture of the modulator will appear to be very long after being scanned by the polygon. The length of the total scanned aperture is determined to be:

DISPLAY IMAGE SIZE

$$2L_1 \tan\left(\frac{\theta_2}{2}\right) = x_1$$

The final image size is just the demagnification of the scanned aperture:

$$\frac{x_1}{D_{mag}} = x_3$$

OUTPUT LENS

The f-number of the output lens is typically very small, e.g. 0.25-1. These values are difficult and expensive to achieve with refractive lenses, but typical in reflective optics.

The output f-number is given as:

$$\frac{x_3}{L_2} = f_{num}$$

POLYGON SCAN RATE

The polygon has historically placed tight constraints parameters of a Scophony style scanned aperture electroholography system but these constraints are loosened somewhat in our case. In the earlier work on this geometry [21] the polygon was identified as problematic because it would be required to become very large and rotate very quickly as the display scaled. However we have the option of adding more device channels as the display scales to reduce the required scanning speed or oversampling. In fact for a very large display we can make one channel for every vertical line of output so that we need only 30 facets to be scanned in a second. For a 6 sided polygon that corresponds to 5 revolutions per second or 300 revolutions per minute. Polygons with more facets would allow for even slower rotations.

Inexpensive, mass-produced polygons typically have six sides (and therefore a 120 degree sweep) and a 20mm facet. It's maximum rotation rate is between 6000 and 16000 rotations per minute(RPM). This gives 150 and 270 rotations per second which give 900 to 1600 facets per second. I ended up choosing a relatively low speed, 7800 RPM to keep noise down.

SCAN PERIOD

The scan period is the time it takes for the polygon to scan the modulator aperture. This parameter will limit the frame rate and display resolution per modulator channel.

The period is given as:

$$\frac{1}{v} = \tau$$

FRAME RATE

Usually you will want to choose a video framerate such as 30 or 60hz (it would be difficult to claim that you're doing holovideo otherwise). However it can be helpful, before scaling up a display for example, to reduce the frame rate to 10Hz or less to allow for increased vertical resolution. Vertical resolution makes a big difference in the output image quality especially for resolutions below 500 vertical lines.

DISPLAY VERTICAL RESOLUTION

The vertical resolution follows from the equation:

$$\frac{v}{fps} = N_{res}$$

SAW VELOCITY

Previous work on the MIT holovideo architectures has made a priority out of descanning the acoustic wave pattern at the acoustic velocity in the crystal. However it may be sufficient to descann the modulation pattern on top of the acoustic wave carrier. Imagine, for example, that instead of writing an acoustic pixel, moving to the next position and writing the next acoustic pixel, that we stayed in one position and wrote one pixel, and then overwrote that pixel with the next pixel several times before moving to the next position. If the consecutive pixels were the same there would be no change in the holographic pattern and one could choose the speed of the descann independently of the acoustic wave speed. However, the cost of this extra flexibility would be the wasting of the bandwidth in our precious bandwidth budget unless we used the re-writing of acoustic pixels as a way to increase dynamic range.

OVERSAMPLING

I will call the re-writing of acoustic pixels, 'oversampling', require that it always be greater than one and define it as follows:

$$\frac{\tau V_{SAW}}{x_1} = O$$

EXAMPLES

Now that we have the methodology for creating holovideo displays, let's look at three design examples which seek to occupy a different place in the display space by minimizing the display cost, meeting the requirements for a computer monitor and maximizing the display size respectively.

MINIMAL DISPLAY

It is worth asking the question, "What is the minimum cost of getting any kind of holographic display with the technology presented in this dissertation." The answer to this question establishes the new threshold to entry for holographic video research. The least expensive display would be based on a single channel device and have the following characteristics:

LARGE DISPLAY

Guided wave devices can be made to have many channels, in fact, these devices can be made to have a channel for every horizontal line in the display output (500 lines, 1000 lines or more). Assuming we could drive such a display, what might be its geometric parameters?

DESIGN SUMMARY

Now I will summarize the target parameters of the display as well as give a brief overview of the expected electrical, optical, and software paths in the display.

ELECTRICAL PATH

DISPLAY PARAMETERS

Parameter	Small Display	Large Display
Facet size, x_2 :	20 mm	300 mm
View angle, θ_3 :	50 degrees	50 degrees
Modulator angle, θ_1 :	5 degrees	5 degrees
First focal length, L_1 :	229 mm	3,436 mm
Demagnification ratio, D_{mag} :	10	10
Second focal length L_2 :	23 mm	344 mm
Polygon facet number, N_{poly} :	6	6
Polygon scan angle, θ_2 :	120 degrees	120 degrees
Total scanned aperture, x_1 :	793 mm	11,901 mm
Display image size, x_3 :	79 mm	1,190 mm
Output lens f-number, f_{num} :	0.35	0.35
Polygon scan rate, v :	800	30
Polygon scan period, τ :	0.00125 sec.	0.033 sec.
Frame rate, fps :	30	30
Vertical resolution, N_{res} :	26.6 (x18=480)	1 (x480)
Foreshortened SAW velocity, V_{SAW} :	650 m/s	650 m/s
Oversampling, O :	1.02	1.82

Figure 4-8 Large and small example display geometries

This chart gives two sets of parameters, one for a small desktop monitor capable being driven by a single PC and another, larger geometry, which represents the case where every waveguide channel is responsible for only one horizontal line of output.

GPU signals will be mixed and then amplified before entering the guided wave modulator. The GPU will provide an hsync signal that will be divided down to drive the polygon. The GPU will also provide a vsync which will be used in concert with the divided down hsync signal to create a ramp to drive a galvanometric scanner through its angular range once every frame to address each horizontal line. As a polygon facet will scan, the vertical scanner will make one step up the ramp. Another polygon facet will scan defining another horizontal line and the vertical scanner will step up the ramp again until it reaches the end of the ramp, returns to its initial position and the frame is completed.

Holovideo Monitor Electrical System

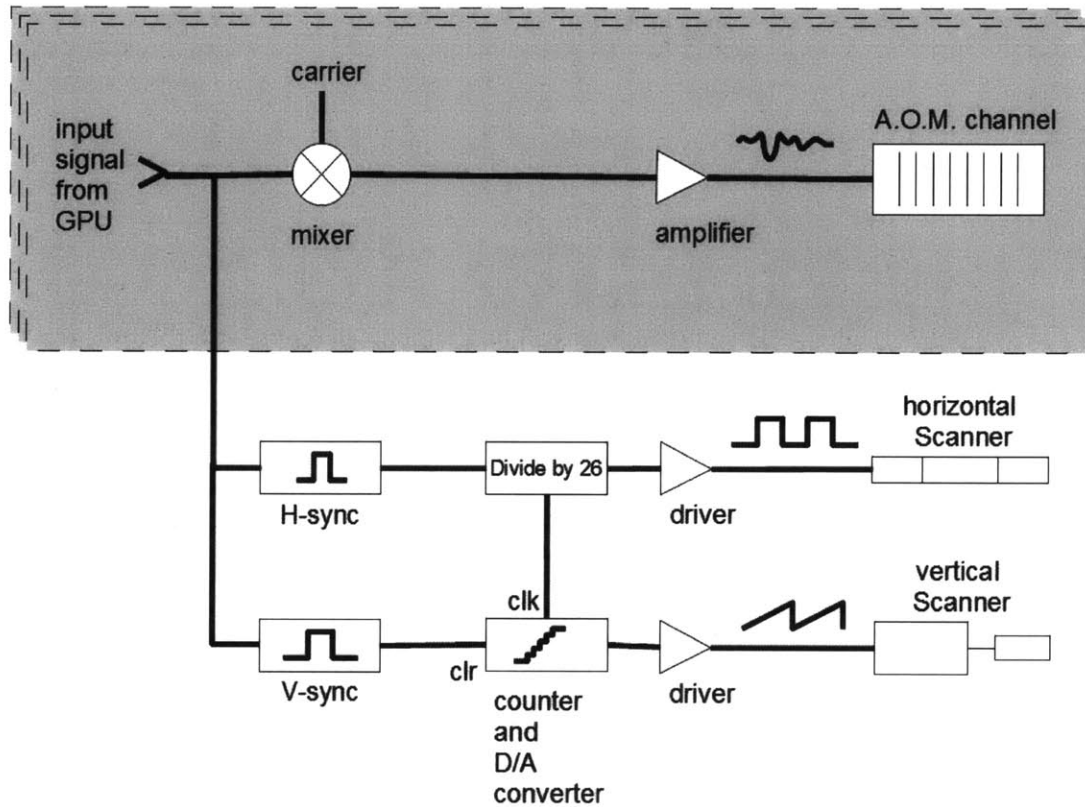


Figure 4-9 Signal path for holovideo monitor electro-optics.

The graphic above gives the signal paths for the electro-optics in my holographic video monitor. With the exception of the modulator, the holographic video monitor's geometry is based off of the layout of the original Mark I holovideo system. This chart is a slightly modified version of the one which describes the Mark I holovideo display in Pierre St. Hiliare's doctoral dissertation [21].

OPTICAL PATH

The optical path will be a simple telescope with the polygon face and galvo as near as possible to the Fourier plane. Optionally, a vertical spatial filter may be added to eliminate noise from waveguide loss.

SOFTWARE PATH

The software driving the display will either load fully computed analytic holograms from memory for static display, or generate holographic patterns in realtime using chirps calculated in the fragment shader of the OpenGL pipeline using a DHCP algorithm [26].

DESIGN SUMMARY

Holographic Video Monitor Optical Path

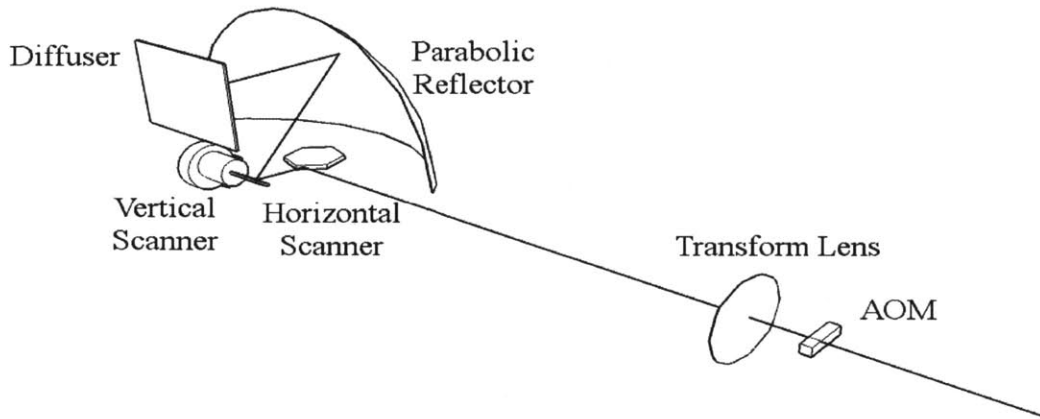


Figure 4-10 Holographic video monitor optical path

The holographic video monitor's optical path differs from that of the Mark I in that it uses a parabolic reflector, instead of a refractive optic, for the output lens (as suggested by Pierre St.-Hilaire).

The completed holographic video monitor should have a form factor similar to an old CRT (cathod ray tube) monitor. It should be fit on a desktop and have an output about screen the size of a post-card. The parts are largely mostly commodity optics and electronics. The chassis will be composed of bent aluminum for lightness, strength and good heatsinking.

Now on to fabrication...

PARTS	
a	power supply
b	chassis
c	first surface
d	transform
e	modulator
f	laser
g	DVI input cards
h	polygon clock/driver
i	first surface
j	first surface
k	polygon mirror
l	galvonometer
m	parabolic mirror
n	vertical diffuser

Holovideo Monitor Internals

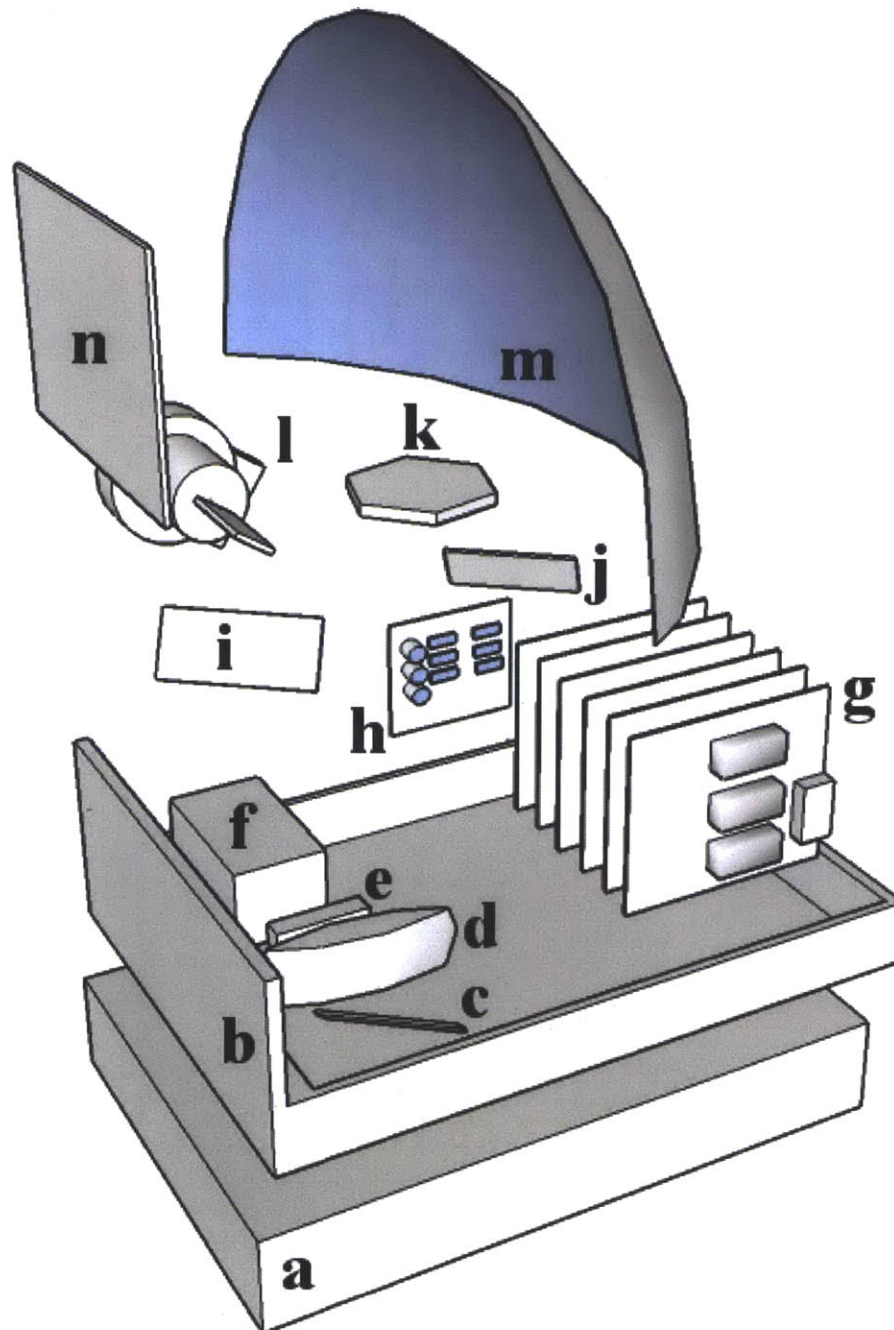


Figure 4-11 Holographic video monitor internals

D E S I G N

64

5

Fabrication

F A B R I C A T I O N

The following chapter is intended not only to document what I did for my dissertation work, but also to provide instructions on how to build a holographic display. Therefore, in a break from the style of previous chapters, this section is written with imperatives and in the present tense.

WAVEGUIDE FABRICATION

The anisotropic leaky mode modulator, or guided-wave device, is the fundamental building block of our holographic display so I will describe its fabrication first.

To make a guided-wave device, you first create waveguides through proton exchange of a lithium niobate surface and then fabricate interdigital transducers. Figure 5-1 shows the steps for proton exchanging a waveguide, and Figure 5-2 shows the steps for creating interdigital transducers.

WAFER CLEANING

Clean the wafer in a 1:1:3 ammonium hydroxide, hydrogen peroxide and water solution at 80 °C for 15 minutes) and then rinse the wafer with deionized (DI) water or isopropanol. In my experience, isopropanol will not leave residue on the front surface of the wafer as it dries. It is more difficult to get DI water to dry cleanly.

(From this moment on there will be a clean side of the wafer and a dirty side of the wafer. Take note of the orientation of the wafer and be sure to process the wafer with the same side up. Choose a preferred orientation for the flats and always process with the wafer in that orientation.)

I used 1mm and 3mm double-side polished x-cut lithium niobate. Crystal technology supplied the 1 mm thick wafers and Del Mar Photonics supplied the 3 mm thick wafers.

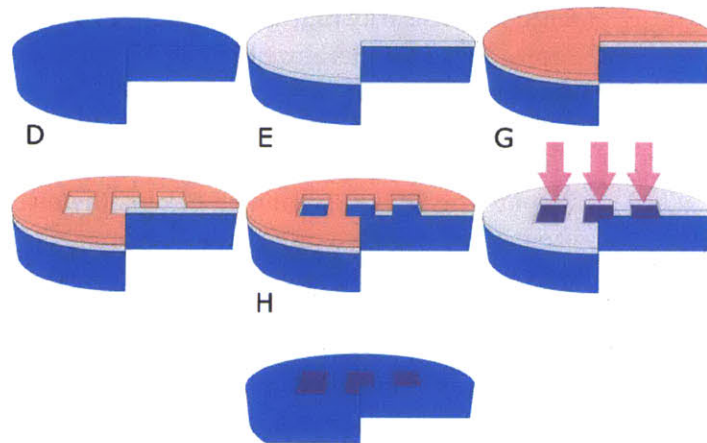


Figure 5-1 Proton exchange of waveguides

A waveguide is formed by taking a clean substrate, depositing silicon dioxide, depositing resist, patterning that resist, etching the silicon dioxide, immersing the substrate in acid and then removing the silicon dioxide.

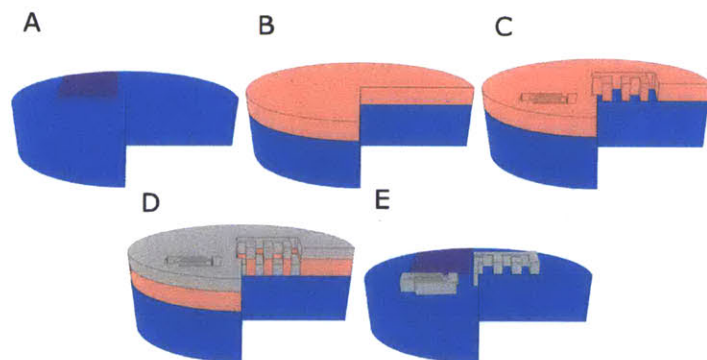


Figure 5-2 Lift-off of aluminum transducers

Transducers are fabricated on a proton exchanged substrate by depositing resist, patterning that resist, depositing aluminum and then removing the resist with a solvent which 'lifts' off the unwanted aluminum leaving transducers.

DEPOSIT SiO_x

The next step is to deposit SiO_x (an amalgum of SiO and SiO₂) on the wafer by physically enhanced chemical vapor deposition (PECVD). In this step, and all others, try to avoid any temperature gradients in time or space which will cause lithium niobate to crack. To avoid wafer fracture, reduce the platen temperature to 100 °C or less. This temperature will provide films of sufficient quality to serve as an etch mask, without endangering the substrate with unnecessarily high temperatures. You may also reduce the shower head temperature to <100 °C but note that this will reduce the deposition rate.

SPIN RESIST

Prepare the SiO_x surface with hexamethyldisilazane, (HMDS) and then apply negative resist, (e.g. Futurrex NR81000P) and spin the wafer at 3000 rotations per minute (kRPM) for 1 minute. Bake the wafer in an oven at 100 °C for 7 minutes to drive off solvents. The bake time is a critical parameter for sidewall shape and for resist development time. Do a matrix of exposures with a dummy wafer to determine the optimum bake time.

PATTERN RESIST

Expose the waveguide pattern using a light-field mask (soda lime glass is fine) with i-line (365 nm) light using contact lithography. Develop the resulting pattern with 2% tetramethylammonium hydroxide (TMAH) solution until the pattern clears (stops changing color) and then rinse in DI water. The development process should take about 1 minute and 40 seconds.

ETCH SiO_x

Dip the wafer in buffered hydrofluoric acid (called buffered oxide etch) for 30 seconds (critical) and then immerse immediately in a water bath. Remove the remaining resist with acetone and clean with methanol and IPA.

PROTON EXCHANGE

You may die saw the wafer at this point into individual devices.

Clean and then immerse the samples in a melt of benzoic acid with a small amount (1% by weight) of lithium benzoate. The immersion time is very sensitive to the amount of lithium benzoate in the melt. Immerse for approximately 90 minutes at 237 °C for single color devices; 1 hr to 4 hrs or more for multiple color devices.

STRIP SiO_x

Strip remaining SiO_x in buffered hydrofluoric acid for 30 seconds or more.

ANNEALING

Heat the sample in a furnace for 45 minutes at 375 °C to anneal the substrate (to mitigate some of the negative effects of proton exchange on the material properties in the waveguiding regions).

SPIN PMMA

Clean the sample. Spin on 600 nm PMMA baked at 150 °C in an oven for 15 minutes. Spin on a conductive layer such as ESpacer (from Showa Denko), Aquasave (from Mitsubishi Rayon) or, alternatively, you can deposit a 20 nm layer of chrome by electron beam evaporation.

PATTERN TRANSDUCERS

Use a scanning electron microscope (SEM), outfitted for patterning, to direct-write transducer patterns at a dose of 275 uC/cm² at a tension of 30 keV using the smallest available spot size and largest current available (aperture) for that spot size. You may also want as large a working distance and field size as possible.

DEVELOP PMMA

Remove the conductive layer with water (for Aquasave or ESpacer) or by chrome etch for chrome. Develop PMMA in a 2:1 Solution of IPA:MIBK (methylisobutylketone) for approximately 30 seconds and check the pattern for adequate development.

DEPOSIT ALUMINUM

Deposit 200nm of aluminum by electron beam evaporation.

POLISH

Polish the exit face of the devices on a lapping polishing tool down to a 0.3 micron grit.

PACKAGE

To package the finished device, mount the chip on a glass slide using a piece of scotch tape on the top surface. Wirebond the SAW transducers to a copper PCB containing a lumped-element matching network. For reference, a typical device might require 40 nH series inductor followed by a shunt capacitance of 2 pF, though these values will vary significantly for different device designs. Matching should be done with the help of a network analyzer to bring the packaged device as close as possible to 50 Ohms impedance.

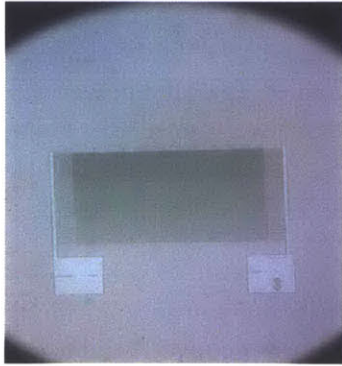


Figure 5-3 A single, chirped transducer

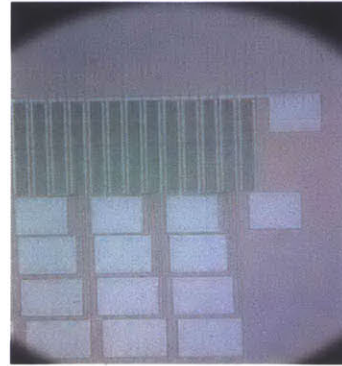


Figure 5-4 Eighteen chirped transducers

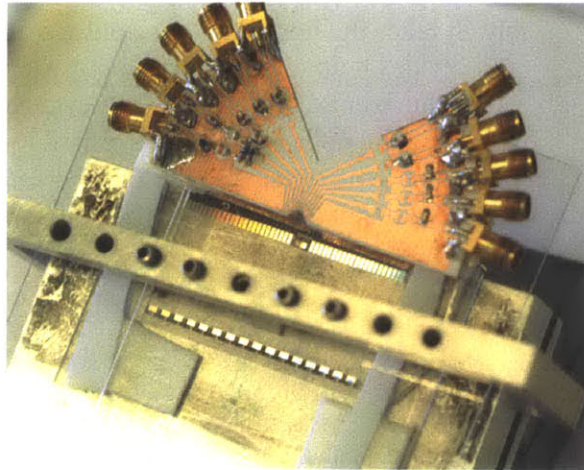


Figure 5-5 A completed guided-wave modulator

DISPLAY FABRICATION

With the guided-wave device completed it is time to construct the supporting geometry. The display is constructed of three basic units: the power supply, the electrical system and the optical system.

POWER SUPPLY

The power supply is composed of a 24 V, 6 Watt switching supply which feeds a number of smaller regulated power supplies assembled from kits (from Nightfire Electronics). The voltages provided are: 24, +18, -18, 12 and 5 V. Also space is allocated for the galvanometric scanner's power supply.

HOLOVIDEO CARD

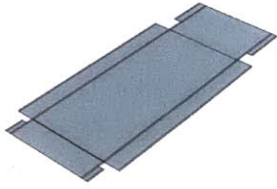
The DVI input card takes the red, green and blue analog video signals from the graphics card and up-converts them to the working frequency of the guided-wave device. To accomplish this, the input signal is mixed with the output of a voltage controlled oscillator (no filtering is done on the signal as the guided wave device act as a filter). The mixer output is pre-amplified and amplified before leaving the card for the guided-wave device.

HORIZONTAL SCANNER CONTROLLER

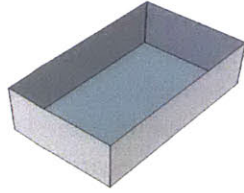
The horizontal scanner controller drives the polygon mirror assembly. It takes the horizontal sync pulse from the analog video signal and divides it down until it has a pulse length that corresponds to one horizontal holo-line. The new holovideo h-sync signal is locked to the polygon by using a phase-locked loop to compare the holovideo sync signal and the signal created by an IR laser bouncing off of the polygon facets. The output is used to drive the polygon motor.

Figure 5-6 Construction of the holographic video monitor (facing page)

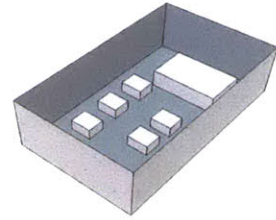
The power supply chassis, and all other chassis, are waterjet cut (a) and folded (b). The power supplies are placed (c) and covered with the main chassis (d). The main chassis is populated with the DVI cards (e) and the lower optics assembly containing the laser and modulator is slid into the main chassis (f). The top chassis with all the scanning electronics is placed (g).



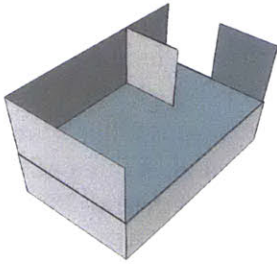
a



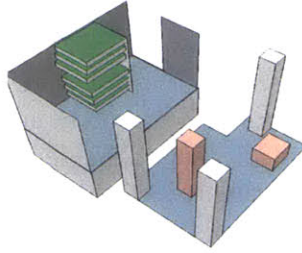
b



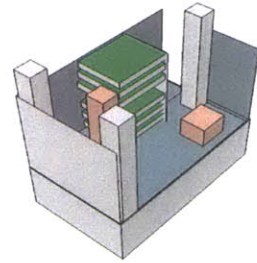
c



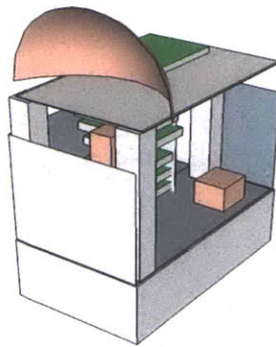
d



e



f



g

VERTICAL SCANNER CONTROLLER

The vertical scanner controller is an Arduino Mega with an external digital to analog converter (DAC). The Arduino and DAC generate a programmable, stepped ramp or triangle signal from the holovideo sync and the analog video v-sync signals. On each holovideo sync pulse, the DAC output voltage increments until the v-sync pulse arrives and the ramp resets. The ramp does not have to reset to zero instantly. It can take one or more holovideo sync pulses to make the transition. This results in less strain and noise in the vertical scanner.

OPTICAL SYSTEM

The optical system couples light into the guided wave device and then scans the output. The optical path begins with a red, green and blue laser on a steel plate. A number of lasers have been used. The most recent display uses a 532nm(80mW) frequency doubled YAG as well as a 638nm(250mW) and 445nm(200mW) diode lasers for a combined power of 530mW. Using three reflectors, the beams are made parallel. The reflectors sit on sliders which allow the spacing of the parallel beams to be adjusted. The beams enter a large diameter cylindrical optic that focuses at the 'wet-spot'(area of frustrated total internal reflection) of an input coupling prism. The prism couples the laser beams into the guided-wave device. The lens acts as a Fourier transform--increasing the distance of the parallel beams from the center of the lens increases the angle at which the beams couple to the guided wave device. In this way different modes can be addressed simply and independently for each color. Mica half-wave plates are used to make sure that the light is of the appropriate polarization. Neutral density filters are used to reduce the light intensity necessary for testing. The output of the modulator exits through a lens which focuses the light onto the polygon face. The path is folded by two mirrors. The light is made to hit the mirror at a slight vertical angle so that when bouncing back there is enough of a difference in height for the output to be picked off

by the vertical scanner which vertically multiplexes the light and directs it towards the parabolic reflector. The vertical focus of the output falls on a vertical diffuser. A polarizer may also be added. Anodized aluminum sheets provide light blocks at various locations.

CHASSIS

The chassis is made from folded sheets of aluminum. This provides stiffness, heat-sinking and RF shielding. The chassis is divided into three modules (listed from bottom to top): the power supply, the guided wave device assembly and the scanning assembly. The chassis is design so that the optical components are part of a rigid frame that can be removed, adjusted, and replaced easily.

COMPLETED DISPLAY

The display is made complete by the addition of a jacket which prevents light leaks, reduces noise and gives the display a monitor-like appearance. The display was designed so that the outer jacket could be interchanged and customized.

Figure 5-7 shows the completed display.

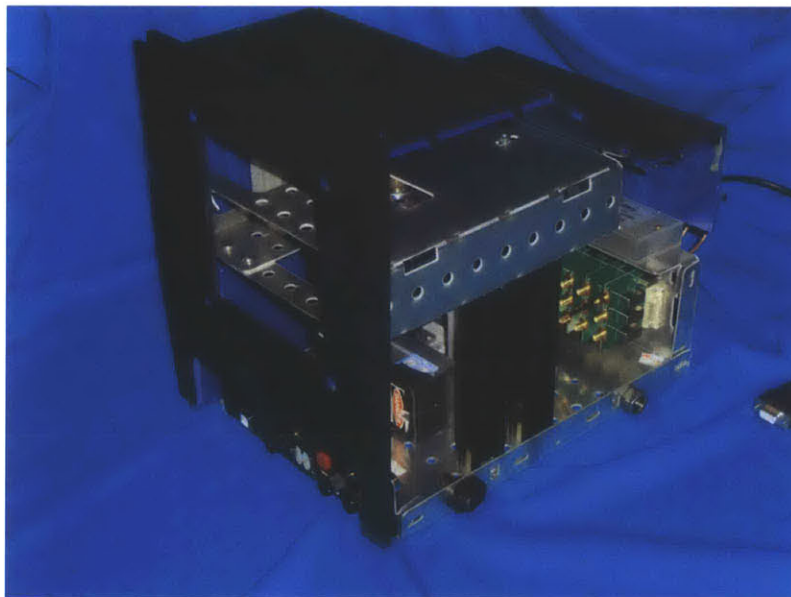


Figure 5-7 The first completed holographic video monitor prototype

D E S I G N

76

6

Results

R E S U L T S

The final implementation of both the waveguide modulator and the holovideo monitor performed largely as expected, however several changes were made which diverged from the design specification. The following chart compares the target design parameters established in Chapter 4 with the results for the final implementation of the guided wave modulator and the holographic video monitor. This chapter gives a description of the expected vs. measured performance and, where changes were made, explains changes were necessary.

SENSITIVITIES

The key parameters for diffraction efficiency from most sensitive to least appear to be: material cut and orientation, channel width, impedance match, proton exchange composition, exchange time and temperature, anneal time and temperature and channel length. The channel width dependency has been included in this thesis (see Figure 6-2). It would be helpful, in future work, to fully isolate and study of each of these parameters.

The key parameters for waveguide loss from most sensitive to least appear to be: proton exchange technique, annealing time (inversely proportional) and waveguide depth. Loss for annealing and waveguide depth are shown qualitatively in Figure 6-3. I chose to present the data in this way because loss measurements on a Metricon prism coupler required fitting a line to some noisy data which, for me, resulted in wide variations in the measured loss for a given sample. More careful use of the Metricon tool or perhaps a modified set of samples optimized for use in the coupler could help.

Figure 6-1 Design parameters vs. measured parameters (facing page)

The design and measured parameters are given, both for the guided wave modulator and for the holovideo display. The parameters that differed greatly from their design values are outlined in red. This design comes from the design summary given in chapter 4 (figure 4-2).

Design vs. Implementation

	Parameter	Design	Implementation
Modulator	Waveguide depth:	1 μm	2 μm
	Coupled Modes:	TE ₁ -TM ₁₁	TE ₂ -TM ₁₂
	Modulator angle, θ_1 :	3 degrees	2.4 degrees
	Channel width:	18 μm	80 μm
	Channel length:	6 and 8 mm	6 and 8 mm
	Number of addressable points/50MHz:	50	30
	Angular sweep/50MHz	3	2.45
Display	Facet size, x_2 :	20 mm	20 mm
	View angle, θ_3 :	30 degrees	24 degrees
	Modulator angle, θ_1 :	3 degrees	2.45 degrees
	First focal length, L_1 :	229 mm	186 mm
	Demagnification ratio, D_{mag} :	10	10
	Second focal length L_2 :	23 mm	19 mm
	Polygon facet number, N_{poly} :	6	6
	Polygon scan angle, θ_2 :	120 degrees	120 degrees
	Total scanned aperture, x_1 :	793 mm	750 mm
	Display image size, x_3 :	79 mm	50 mm
	Output lens f-number, f_{num} :	0.35	0.29
	Polygon scan rate, v :	800	800
	Polygon scan period, τ :	0.00125 sec.	0.00125 sec.
	Frame rate, fps :	30	30
	Vertical resolution, N_{res} :	26.6 (x18=480)	24 (x18=432)
	Foreshortened SAW velocity, V_{SAW} :	650 m/s	650 m/s
Oversampling, O :	1.02	1.02	

RESULTS

WAVEGUIDE DEPTH

I originally anticipated designs with shallow guides for the best overlap between acoustic and optical coupling. However, waveguides don't support mode coupling for red, green and blue until a particular waveguide depth is reached. At present I have no explanation for why this is the case.

COUPLED MODE PAIRS

I initially expected to couple all the modulators from the fundamental or first order waveguide modes and to use the same mode pairs for each color. However, experiments showed that coupling efficiency was better for higher order modes, and the best modes were not necessarily the same for each color.

CHANNEL WIDTH

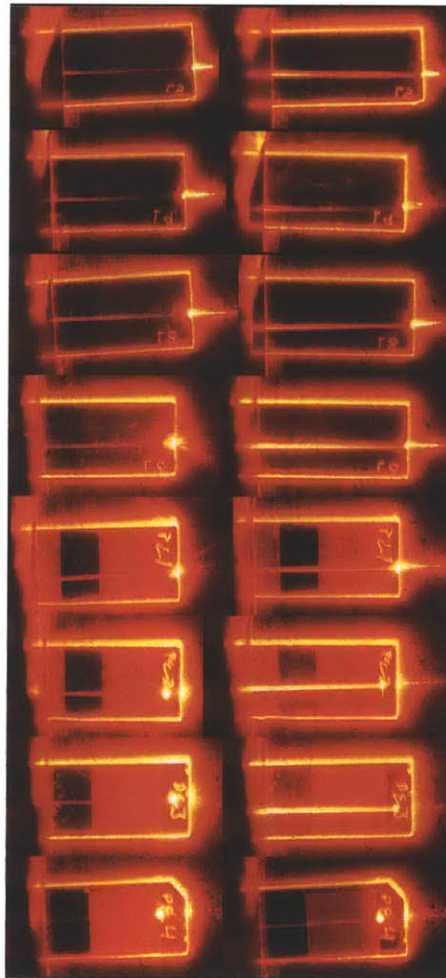
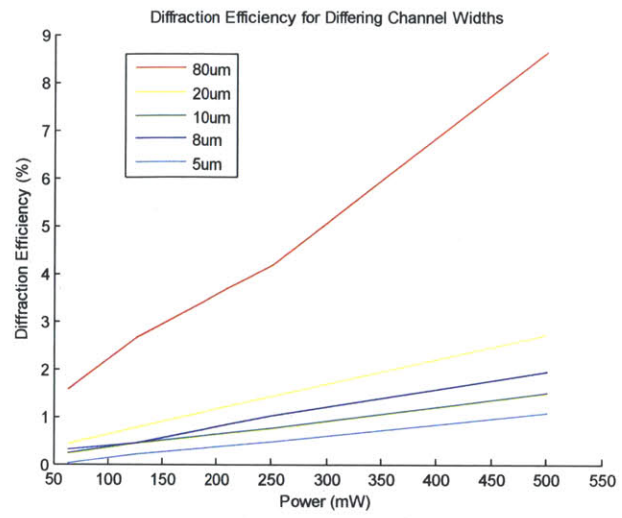
Narrower waveguides should lead to better overlap between acoustic and optical energy and therefore to better efficiency as well. However, in a test of acoustic waveguide coupling efficiency by waveguide depth, the narrow 18 micron channels did not perform as well as wider 80 micron channels. This could be due to different

Figure 6-2 A test of channel width vs. diffraction efficiency (facing page top)

This plot shows mode coupling efficiency vs. channel width. The largest width, 80 microns, which is peculiar because I would have expected the narrowest channel to be most efficient. One possible explanation is that the insertion losses from the parabolic input coupler were the smallest for the 80 micron channel because the channel only had to taper from a 100 micron opening to a 80 micron channel rather than from 100 microns to 40 microns or 20 microns as was the case with the other waveguide channels tested.

Figure 6-3 A test of waveguide loss vs. proton exchange time and annealing(facing page bottom)

The image illustrates a test of waveguide loss vs. waveguide depth for a number of proton exchange times and annealing. Proton exchange times increase from top to bottom. The left hand column contains samples before annealing and the right hand column shows the same samples after annealing. A good quality sample with low loss will have a streak with uniform brightness across the length of the sample and little or no streak at the output. Notice that waveguide quality gets gradually better with exchange time. Notice that waveguide quality is worse for all samples after annealing.



R E S U L T S

input coupling efficiencies and a new experiment which controls for input coupling is a possibility for the future. However, for this dissertation work 80 micron channels were used.

TEST PATTERNS

The central angles of red, green and blue angular sweeps were not, in general, centered. So shifting of the acoustic center frequency of each band was necessary. This was done by aligning crosshair patterns as shown in S 6-11.



Figure 6-4 Test of the telescope demagnification
The image of the, 'f', is demagnified ten times (and inverted) through the telescope.

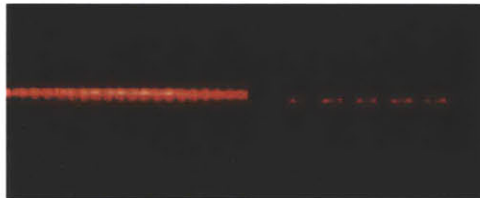


Figure 6-5 Test of image descan
When not descanned a single line of output would look like one continuously moving smear(left). When descanned and stationary, the blanking intervals would appear. through the telescope (right).

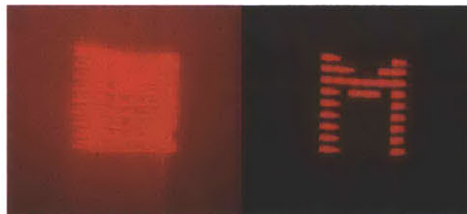


Figure 6-6 Test of the polarization rotation
The scanned output was shown without a polarizer (left) and with a polarizer (right) to exclude noise.



Figure 6-7 One view of a reconstructed holographic stereogram.

This is as it appeared on the holographic video monitor. You may be able to see the curve of the output mirror in the background. The image was 156 lines vertically refreshed at 5Hz and measured approximately 2x3cm at the diffuser.



Figure 6-8 Close up of a monochrome holographic stereogram

OUTPUT IMAGES

These output images demonstrate desmagnification, descanned, polarization rotation, resolution and image size.

WAVELENGTH DIVISION MULTIPLEXING FOR COLOR

The figures on this page illustrate wavelength division for color.

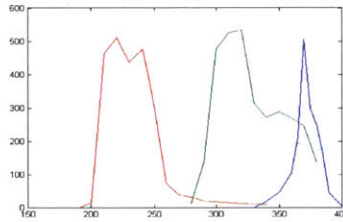


Figure 6-9 Frequency response for device used in holographic video monitor

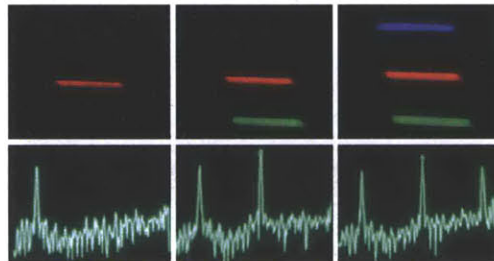


Figure 6-10 Demonstration of frequency division color control

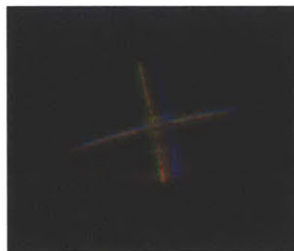


Figure 6-11 Crosshairs used to align the three color images

The differently colored images needed alignment which could be performed by changing the center frequency of each signal. The rotation shown is an artifact of illuminating the polygon off-axis (future prototypes will attempt on-axis illumination).

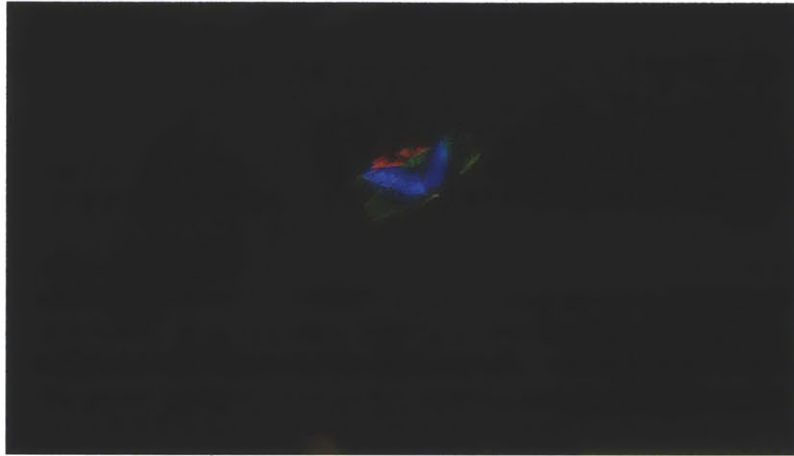


Figure 6-12 Full color holographic stereogram

This stereogram was created by the holographic video monitor with a single channel waveguide modulator employing frequency division of color.

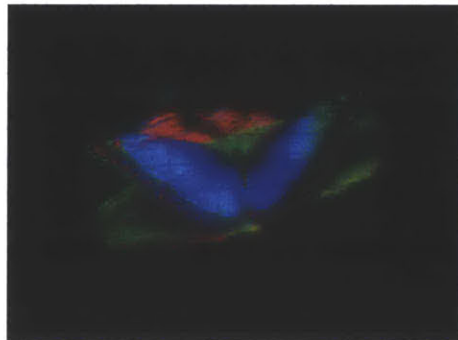


Figure 6-13 Close up of color stereogram

PROBLEMS AND CHALLENGES

Until now the biggest problem with the waveguide devices has been low diffraction efficiency. Now that we have achieved mode coupling efficiency near 10% we turn our attention to overall efficiency and loss at the input coupling stage. Future efforts may make use of inexpensive grating couplers as input devices or may attempt to optimize the gap distance for prism coupling with a goal of achieving 50% or better input efficiencies (currently I get 10% or less coupling efficiency with the rutile prism though little effort has been given to optimizing evanescent coupling.)

The next highest priority item would be increase the number of scannable points to more closely approach the diffraction limit for the device which appears to be lower than desired. This means a careful study of acoustic wave propagation in the waveguides on thick substrates to make sure the out-coupling efficiency is constant along the length of the waveguide channel. It might be helpful to have the surface acoustic waves travel colinearly rather than contralinearly with the guided light.

There is also a need to design a way to effectively extract or extinguish the unmodulated light in the waveguide which currently just exits the edge of the wafer. A simple light block could be used, or perhaps a metalized region on the top of the device to absorb the light energy.

There is a need to explore other proton exchange techniques such as titanium indiffused proton exchange (TIPE) and reverse proton exchange (RPE). Titanium indiffusion allows for the possibility of using Y-cut lithium niobate as a substrate and it would be valuable to see if this cut would be suitable for devices that make use of its higher electromechanical coupling coefficient.

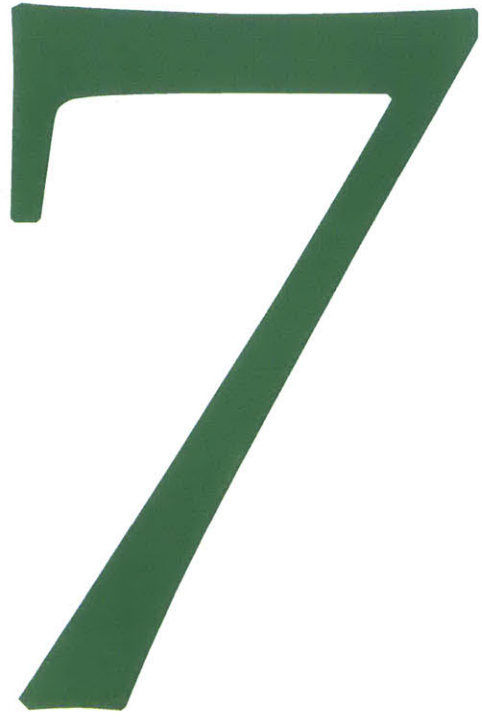
There are several challenges that remain to be overcome including refining the polygon scanner driver circuit to achieve a tighter lock on the polygon scan. At present the best lock still has a jitter of 8-10ns which can give some noticeable movement in the display

output. The current level of lock is achieved almost exclusively with by varying the gain.

It would be interesting to see if a more carefully designed loop filter or PID controller might be able to achieve a better lock, be more resistant to noise, or be able to achieve lock without any real-time adjustment of the loop filter.

R E S U L T S

88



Conclusion

C O N C L U S I O N

In my dissertation proposal I promised to deliver the following:

- A holographic video display based on guided wave devices which is capable of moving images, near standard resolution (~480 vertical lines), 30 Hz refresh and inexpensive construction.
- A detailed description of the fabrication process.
- A demonstration of wavelength division multiplexing for color—with the caveat that blue light operation would be exempted if it proved too difficult.

HOLOVIDEO DISPLAY

I built two and a half holovideo prototypes over the course of this dissertation work. The final prototype has a resolution of 480 vertical lines (435 visible due to blanking) with a 30 degree maximum view-angle and a 30Hz refresh as specified. It uses frequency division of color and employs red, green and blue(!) sources.

DOCUMENTATION

In addition to the Design and Fabrication chapters of this dissertation document (with their associated appendices), I have created training videos that step through the device fabrication process.

WAVELENGTH DIVISION MULTIPLEXING OF COLOR

I have demonstrated, and published about, wavelength division multiplexing of color in anisotropic leaky mode devices.

SUCCESS

I believe I have met the goals set forth in my dissertation proposal. I have introduced a new, low cost platform for holographic video research and instantiated the world's first low-cost, PC-driven holographic video monitor.

FUTURE WORK

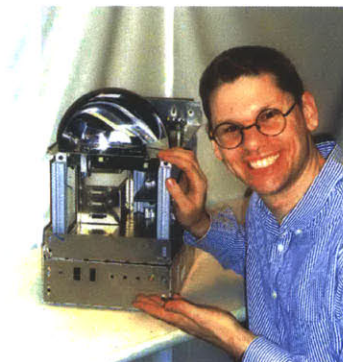
Now that the world has a flexible platform for holographic video research, the next steps are to explore the platform for design nodes that allow: full parallax displays, large displays, solid state displays and deep (high space-bandwidth product) displays. Several of these efforts are already underway.

It is also important that a careful mathematical analysis be done of frequency division multiplexing of color in holographic display with an effort to create a design plot for display designers.

With the introduction of a low cost, PC-controlled holovideo monitor, it is time to explore holographic video desktop applications for security, telepresence, data visualization and entertainment.

CLOSING STATEMENT

When I was a kid I imagined I would one day be making science-fiction a reality using a mixture of junk and cutting-edge laser technology. I hope my nine year-old self would be proud.



C O N C L U S I O N

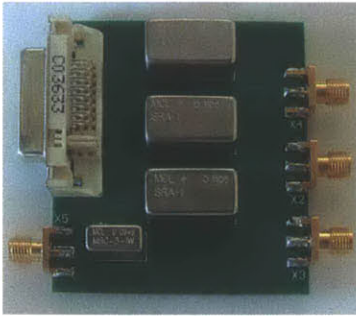
C O N C L U S I O N

92

8

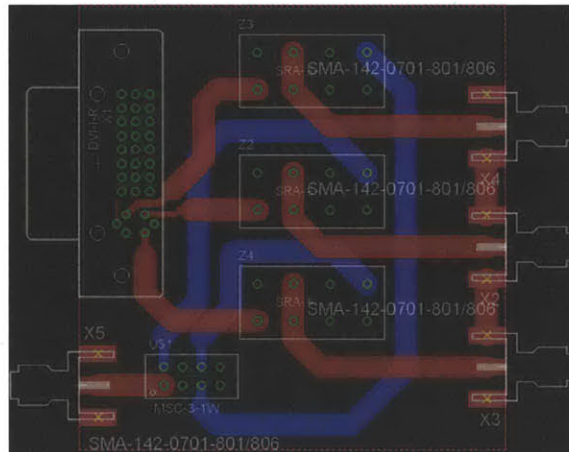
Appendix

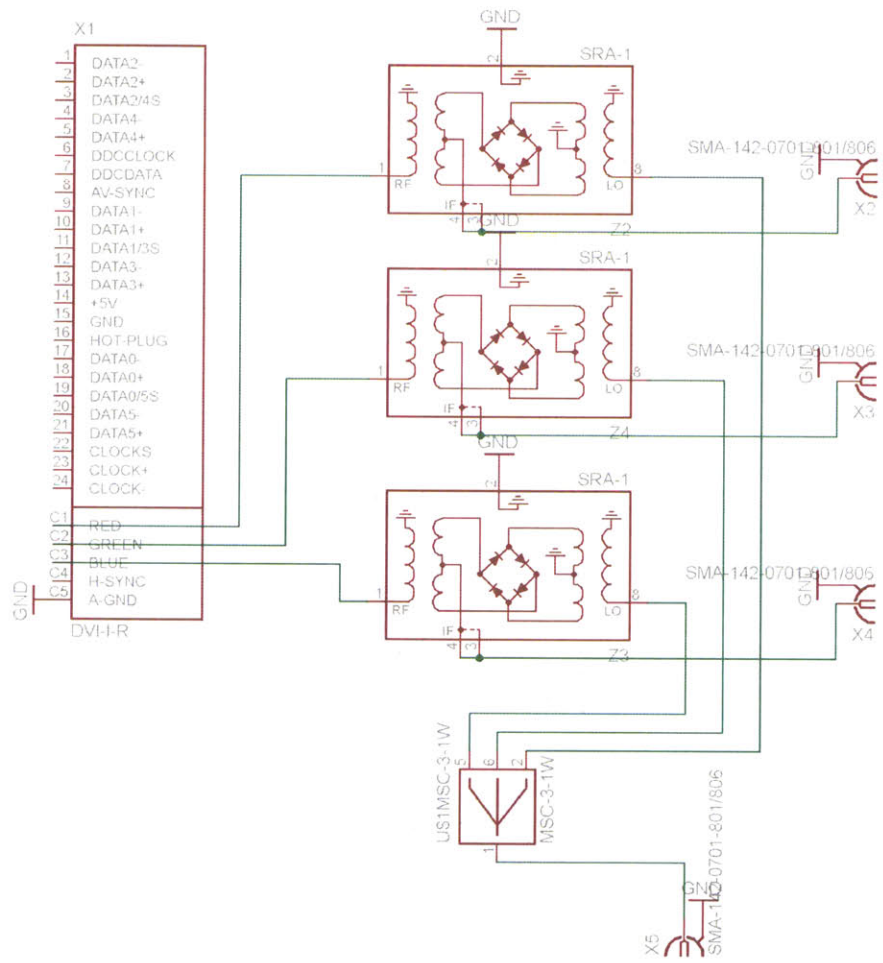
A P P E N D I X

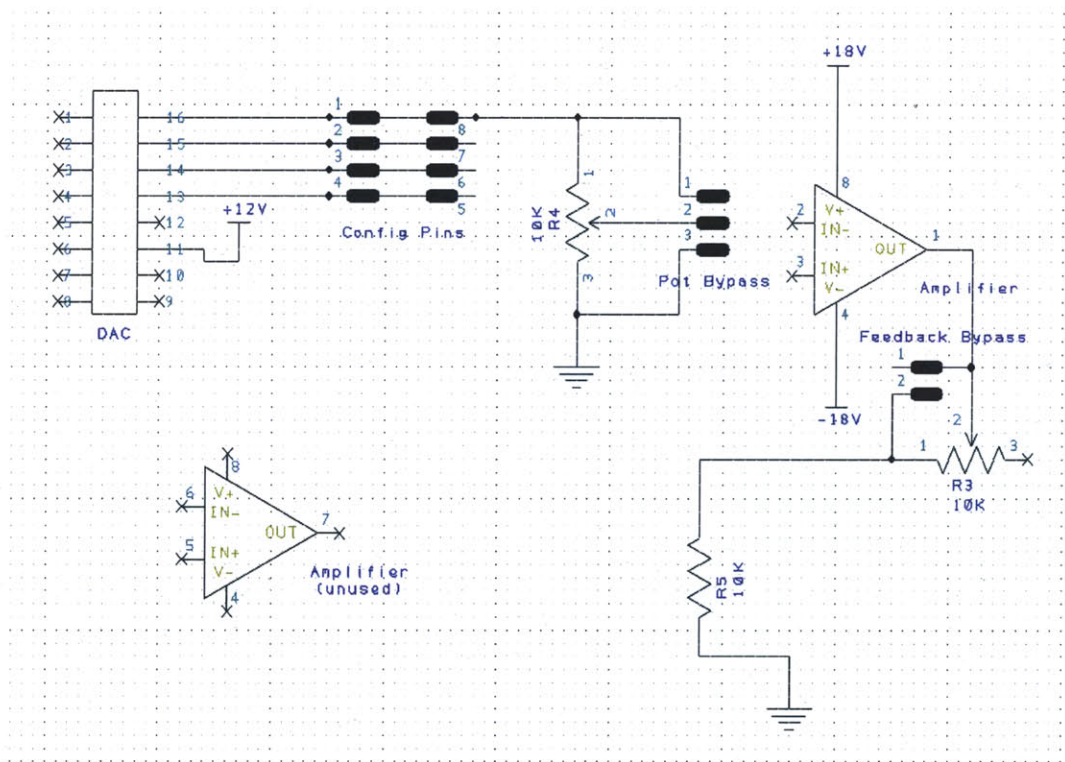


HOLOVIDEO CARD

The schematic and PCB board for the holovideo card is shown below.







A P P E N D I X

100

A P P E N D I X

101

A P P E N D I X

102

A P P E N D I X

103

A P P E N D I X

104



Bibliography

B I B L I O G R A P H Y

- [1] C. S. Tsai, *Guided-Wave Acousto-Optics: Interactions Devices and Applications*. Springer-Verlag, 1990.
- [2] K. Nakamura, J. Miyazu, M. Sasaura, and K. Fujiura, "Wide-angle, low-voltage electro-optic beam deflection based on space-charge-controlled mode of electrical conduction in $KTa_{1-x}Nb_xO_3$," *Applied physics letters*, vol. 89, no. 13, pp. 131115–131115, 2006.
- [3] O. Solgaard, "Integrated semiconductor light modulators for fiber-optic and display applications," Stanford University, 1992.
- [4] Y. Kurosaka, S. Iwahashi, Y. Liang, K. Sakai, E. Miyai, W. Kunishi, D. Ohnishi, and S. Noda, "On-chip beam-steering photonic-crystal lasers," *Nat Photon*, vol. advance online publication, May 2010.
- [5] R. Stahl, V. Rochus, X. Rottenberg, S. Cosemans, L. Haspeslagh, S. Severi, G. Van der Plas, G. Lafruit, and S. Donnay, "Modular sub-wavelength diffractive light modulator for high-definition holographic displays," in *Journal of Physics: Conference Series*, 2013, vol. 415, p. 012057.
- [6] T. Kreis, P. Aswendt, R. Ho, and others, "Hologram reconstruction using a digital micro-mirror device," *Optical Engineering*, vol. 40, no. 6, pp. 926–933, 2001.
- [7] E. Pearson, "MEMs Devices for Holographic Video," MIT, 2001.
- [8] R. Haussler, A. Schwerdtner, and N. Leister, "Large holographic displays as an alternative to stereoscopic displays," in *Proc. SPIE*, 2008, vol. 6803.
- [9] G.-L. Chen, C.-Y. Lin, M.-K. Kuo, and C.-C. Chang, "Numerical suppression of zero-order image in digital holography," *Optics Express*, vol. 15, no. 14, pp. 8851–8856, 2007.
- [10] K. Sato, A. Sugita, M. Morimoto, and K. Fujii, "Reconstruction of color images of high quality by a holographic display," in *Integrated Optoelectronic Devices 2006*, 2006, p. 61360V–61360V.
- [11] J. L. Jackel, C. Rice, and J. Veselka, "Proton exchange for high-index waveguides in $LiNbO_3$," *Applied Physics Letters*, vol. 41, p. 607, 1982.
- [12] Matteo et al., "Collinear Guided Wave to Leaky Wave Acoustooptic Interactions in Proton-Exchanged $LiNbO_3$," *IEEE Transactions on Ultrasonics, Ferroelectrics, and Frequency Control*, vol. 47, no. 1, 2000.
- [13] U. Rust and E. Strake, "Acoustooptical Coupling of Guided to Substrate Modes in Planar Proton-Exchanged $LiNbO_3$ -Waveguides," in *Proceedings of Integrated Photonics Research*, 1992.
- [14] Proklov, "Multichannel Waveguide Devices using Collinear Acoustooptic Interaction," Institute of Radio Engineering and Electronics of the Russian Academy of Sciences, 1992.
- [15] K. Ito and K. Kawamoto, "An Optical Deflector Using Collinear Acoustooptic Coupling Fabricated on Proton-Exchanged $LiNbO_3$," *Jpn. J. Appl. Phys. Vol.*, vol. 37, no. 9A Pt 1, pp. 4858–4865, 1998.
- [16] J. Xu and R. Stroud, *Acousto-optic devices: principles, design, and applications*. Wiley New York, 1992.

- [17] Smith, Richard W., "Analysis of Interdigital Surface Wave Transducers by Use of an Equivalent Circuit Model," IEEE Transactions on Microwave Theory and Techniques, vol. MTT-17, no. 11, 1969.
- [18] M. Solal, V. Laude, and S. Ballandras, "A P-Matrix based Model for SAW Grating Waveguides taking into account Modes Conversion at the Reflection," IEEE Transactions on Ultrasonics, Ferroelectrics and Frequency Control, vol. 51, no. 12, 2004.
- [19] D. Marcuse, "Coupled-mode theory for anisotropic optical waveguides," Bell System Technical Journal, vol. 54, no. 6, pp. 985–995, 1975.
- [20] A. Campari, C. Ferrari, G. Mazzi, C. Summonte, S. Al-Shukri, A. Dawar, R. De La Rue, and A. Nutt, "Strain and surface damage induced by proton exchange in Y-cut LiNbO₃," Journal of applied physics, vol. 58, no. 12, pp. 4521–4524, 1985.
- [21] P. S.-Hilaire, "Scalable Architectures for Holographic Video," MIT, 1994.
- [22] E. Y.-B. Pun, Y. O. Tse, and P. S. Chung, "Proton-exchanged optical waveguides in LiNbO₃ using octanoic acid," Photonics Technology Letters, IEEE, vol. 3, no. 6, pp. 522–523, 1991.
- [23] Y. N. Korkishko, V. Fedorov, T. Morozova, F. Caccavale, F. Gonella, and F. Segato, "Reverse proton exchange for buried waveguides in LiNbO₃," Journal of the Optical Society of America A, vol. 15, no. 7, pp. 1838–1842, 1998.
- [24] M. Miyawaki and S. Ogura, "Efficient, Damage resistant LiNbO₃ acousto-optic waveguide deflector," Applied Physics Letters 49, 16- (1986), 1986.
- [25] V. Hinkov, R. Opitz, and W. Sohler, "Collinear acoustical TM-TE mode conversion in proton exchanged Ti: LiNbO₃ waveguide structures," Lightwave Technology, Journal of, vol. 6, no. 6, pp. 903–908, 1988.
- [26] Q. Y. J. Smithwick, J. Barabas, D. E. Smalley, and V. M. B. Jr, "Interactive holographic stereograms with accommodation cues," 2010, vol. 7619.
- [27] C. S. Tsai. *Guided-Wave Acousto-Optics: Interactions Devices and Applications*. Springer-Verlag, 1990.
- [28] Slobodnik Jr, A. J., and E. D. Conway. *Microwave Acoustics Handbook. Volume 1. Surface Wave Velocities*. No. AFCRL-PSRP-414. Air Force Cambridge Research labs Hanscom AFB MA, 1970.
- [29] Caballero-Calero, O., et al. "Optical damage in x-cut proton exchanged LiNbO planar waveguides." *Journal of applied physics* 100 (2006): 093103.
- [30] J.A. deToro, M.D. Serrano, A.G. Cabanes, J.M. Cabrera [*Opt. Commun. (Netherlands)* vol.154 (1998) p.23]
- [31] L.P. Avakyants, D.F. Kiselev, N.N. Shchitov [*Sov. Phys.-Solid State (USA)* vol.6 (1976) p.899]
- [33] Sun, Jie, et al. "Large-scale nanophotonic phased array." *Nature* 493.7431 (2013): 195-199.
- [34] Tsai, Chen S., and David Young. "Magnetostatic-forward-volume-wave-based guided-wave magneto-optic Bragg cells and applications to communications and signal processing." *Microwave Theory and Techniques, IEEE Transactions on* 38.5 (1990): 560-570.